

UCLA

UCLA Previously Published Works

Title

Network Analysis in Disorders of Consciousness: Four Problems and One Proposed Solution (Exponential Random Graph Models)

Permalink

<https://escholarship.org/uc/item/4c55d97f>

Journal

Frontiers in Neurology, 9(JUN)

ISSN

1664-2295

Authors

Dell'Italia, John
Johnson, Micah A
Vespa, Paul M
[et al.](#)

Publication Date

2018

DOI

10.3389/fneur.2018.00439

Peer reviewed

Network analysis in disorders of consciousness: four problems and one proposed solution (Exponential Random Graph Models)

John Dell'Italia^{1,*}, Micah A. Johnson¹, Paul M. Vespa², Martin M. Monti^{1,2}

¹*Department of Psychology, University of California Los Angeles, Los Angeles, CA, USA*

²*Brain Injury Research Center (BIRC), Department of Neurosurgery, David Geffen School of Medicine at UCLA, Los Angeles, CA, USA*

Correspondence*:

John Dell'Italia, Department of Psychology, University of California Los Angeles, Los Angeles, CA 90095
johndellitalia@ucla.edu

2 ABSTRACT

3 In recent years, the study of the neural basis of consciousness, particularly in the context
4 of patients recovering from severe brain injury, has greatly benefited from the application of
5 sophisticated network analysis techniques to functional brain data. Yet, current graph theoretic
6 approaches, as employed in the neuroimaging literature, suffer from four important shortcomings.
7 First, they require arbitrary fixing of the number of connections (i.e., density) across networks
8 which are likely to have different “natural” (i.e., stable) density (e.g., patients vs controls, vegetative
9 state vs minimally conscious state patients). Second, when describing networks, they do not
10 control for the fact that many characteristics are interrelated, particularly some of the most popular
11 metrics employed (e.g., nodal degree, clustering coefficient) – which can lead to spurious results.
12 Third, in the clinical domain of disorders of consciousness, there currently are no methods for
13 incorporating structural connectivity in the characterization of functional networks which clouds
14 the interpretation of functional differences across groups with different underlying pathology as
15 well as in longitudinal approaches where structural reorganization processes might be operating.
16 Finally, current methods do not allow assessing the dynamics of network change over time. We
17 present a different framework for network analysis, based on Exponential Random Graph Models
18 (ERGM), which overcomes the above limitations and is thus particularly well suited for clinical
19 populations with disorders of consciousness. We demonstrate this approach in the context of
20 the longitudinal study of recovery from coma. First, our data show that throughout recovery
21 from coma, brain graphs vary in their natural level of connectivity (from 10.4% to 14.5%), which
22 conflicts with the standard approach of imposing arbitrary and equal density thresholds across
23 networks (e.g., time-points, subjects, groups). Second, we show that failure to consider the
24 interrelation between network measures does lead to spurious characterization of both inter- and
25 intra-regional brain connectivity. Finally, we show that Seperable Temporal ERGM (STERGM) can

26 be employed to describe network dynamics over time revealing the specific pattern of formation
27 and dissolution of connectivity that accompany recovery from coma.

28 **Keywords:** Network Analysis, Exponential Random Graph Model, functional Magnetic Resonance Imaging, Coma, Disorders of
29 Consciousness

1 INTRODUCTION

30 In the past 15 years, in vivo studies of the healthy and diseased brain have increasingly focused on
31 approaches aimed at assessing the spontaneous functional architecture of the brain, conceived as a network
32 of interacting regions (Raichle et al., 2001). Network analyses have been successfully employed in many
33 fields, including sociology (Freeman, 1978), computer sciences (McQuillan, 1977), public health (Luke
34 and Harris, 2007), epidemiology (Lucek and Ott, 1997) and transportation (Guimera et al., 2005), among
35 others, to capture salient aspects of each phenomenon. Indeed, while different fields often employ different
36 approaches to assessing network properties, they all share the common goal of characterizing important
37 aspects of complex network function into a limited number of metrics, which can, jointly, capture both what
38 is unique and what is shared across systems. Network approaches have also been extensively employed
39 towards understanding specific aspects of cognition (e.g., Cao et al., 2014), development (Fransson et al.,
40 2010) and aging (Micheloyannis et al., 2009), and, perhaps most frequently, the pathological brain (e.g.,
41 Alzheimer's disease; Sanz-Arigita et al., 2010, Parkinson disease; Wu et al., 2009, severe brain injury;
42 Pandit et al., 2013). This approach has also found fruitful application in the study of human consciousness
43 (e.g., Monti et al., 2013; Chennu et al., 2014; Crone et al., 2017b). Indeed, many of the proposals of
44 how human consciousness arises from neural function often make reference to aspects of brain activity
45 as a network of interacting areas, such as the reverberation and spread of neural activity across fronto-
46 parietal association regions (Baars, 2002; Baars et al., 2003), the presence of synchronized long-range
47 activity in specific frequency bands (e.g., Engel and Singer, 2001; Tallon-Baudry, 2009) and specific
48 neural circuits (e.g., cortico-thalamic loops; Dehaene and Changeux, 2005), the dynamic competition
49 between assemblies of cells (Crick and Koch, 2003), or to the degree to which a network possesses certain
50 topological characteristics (e.g., integration and differentiation; Tononi, 2008).

51 In the context of disorders of consciousness (DOC; Monti et al., 2010), network approaches to the
52 study of functional connectivity have given rise to a fertile body of literature (see Hannawi et al., 2015,
53 for a recent review). Yet, there are a number of important methodological challenges which might play
54 into the interpretation of such studies (cf., Soddu et al., 2011; Boly et al., 2012a) and which might explain
55 some of the contrasting results reported (e.g., the exact role of thalamo-cortical versus cortico-cortical
56 connectivity in recovery of consciousness; see Laureys et al., 2000a,b; Vanhaudenhuyse et al., 2010; Boly
57 et al., 2009, 2011; Crone et al., 2014; Amico et al., 2017; Crone et al., 2017a). (See also Monti (2012) for
58 further discussion).

59 In what follows, we propose that it is best to have both seed based and graph theoretic questions in a
60 single model. In the neuroimaging literature, there are a number of limitations of current approaches which
61 have hindered the ability to use a single model for combining seed based and graph theoretic approaches,
62 but there are models that have been developed by other fields (Holland and Leinhardt, 1981; Hunter, 2007;
63 Hunter et al., 2008; Goodreau et al., 2009; Handcock et al., 2017).

64 1.1 Four problems in current network analysis approaches

65 Current graph theory methods as employed in neuroimaging (Bullmore and Sporns, 2012; Rubinov
66 and Sporns, 2010) suffer from a number of important shortcomings which are particularly relevant in the
67 domain of disorders of consciousness. (We note that the following discussion is in the context of network
68 analysis as currently implemented for neuroimaging data, and is not meant to imply that other fields have
69 not found solutions to them. In fact, as we will argue below, we are advocating for importing into the field
70 of neuroimaging methods that have successfully been applied in other domains.)

71 1.1.1 Problem #1: Arbitrary enforcing of network density

72 Conventional graph theoretic approaches in neuroimaging require sparse networks. That is to say,
73 they require networks (i.e., connectivity matrices) to have some connections (i.e., edges) with non-zero
74 values (typically integer, in binary networks, or fractional, in weighted networks) and some with zero
75 values – as opposed, for example, to fully connected networks in which all edges have non-zero values
76 (i.e., each node is connected to all other nodes with non-zero edges). Yet, since brain networks are typically
77 derived from pairwise correlations across time-series of regions of interest, the starting point for network
78 analysis is typically a fully connected network (in fact, a complex network, which is both fully connected
79 and has positive and negative edges; Rubinov and Sporns, 2011). It is thus common procedure to make
80 the connectivity matrices sparse by fixing their density (i.e., the proportion of non-zero edges to the total
81 number of possible edges), which is done by retaining the strongest d connections and setting all remaining
82 ones to zero. The resulting network is thus sparse, with density $\frac{d}{N(N-1)/2}$, where N is the number of nodes
83 in the network. On the one hand, this procedure ensures that any uncovered difference across networks (e.g.,
84 patients vs volunteers; time-point A vs time-point B) reflects some systematic aspect of their topological
85 characteristics and not, more trivially, the fact that they have different densities. On the other hand, however,
86 because of the lack of a principled approach to perform this procedure, it is currently typical to iteratively
87 re-calculate network characteristics at several density levels, from a lower bound meant to ensure that
88 networks are estimable (such that the average nodal degree is no smaller than $2 \times \log(N)$; Watts and
89 Strogatz, 1998) to an upper bound such that the mean small-world characteristic of networks is no smaller
90 than 1 or 1.5 (e.g., Monti et al., 2013). While conventional, the idea of enforcing graphs to have the same
91 density across groups, time-points, or conditions is in itself problematic, because it is not hard to imagine
92 that some graphs might be naturally denser than others (see Nielsen et al., 2013). This is particularly
93 relevant in the context of the typical comparisons of interest in disorders of consciousness such as patients
94 versus healthy volunteers, patients in a Vegetative State versus patients in a Minimally Conscious State
95 (versus patients in a Locked-in Syndrome), or within-patient changes over time (e.g., acute-to-chronic
96 designs). Of course, similar problems are encountered in many other contexts (e.g., adolescents versus
97 older adults) and might even apply to normal, within-group, variability in the healthy brain. Mandating
98 equal density across graphs might obscure important differences across conditions of interest, bias results,
99 and lead to spurious findings.

100 One solution to the problem of network iterative thresholding is to analyze complex networks (i.e.,
101 fully connected and signed matrices; Rubinov and Sporns, 2011; Fornito et al., 2013, 2016). Yet, despite this
102 problem having been well documented, as shown in a recent review focused on the use of graph-theoretic
103 approaches in the clinical context, less than 7% of 106 published papers (up to April 2016) employed
104 complex matrices (Hallquist and Hillary, 2018). All remaining studies only considered non-negative and/or
105 sparse matrices. In addition, it is important to note two potentially unwanted limitations of using complex
106 matrices. First, complex matrices assume that the probability of connectivity between two regions is

107 spatially stationary, but it is in fact well known to be inversely related to distance at both the neuronal and
108 region levels (see Hellwig, 2000; Averbach and Seo, 2008; Braitenberg and Schüz, 1998). Second, the
109 use of complex matrices affects the formulation of some metrics (e.g., modularity; Rubinov and Sporns,
110 2011; Fornito et al., 2013) because positive and negative edges are treated as separate sparse networks,
111 an issue that is further complicated by the use of mean-centering preprocessing strategies CITE LAST
112 POWERS which are known to shift the distribution of positive and negative edges CITATION. Furthermore,
113 the formulation and interpretation of other metrics (e.g., path based metrics such as characteristic path
114 length/local efficiency, betweenness centrality, etc.; Fornito et al., 2013; Wang et al., 2017), are also
115 affected since the weights represent both the strength and probability of the connections (i.e., density).
116 Thus, analyzing fully connected signed graphs does avoid the thresholding issue but at the cost of clouding
117 the interpretation of metrics such as density and path-based graph statistics.

118 1.1.2 Problem #2: Network measures are not independent of each-other

119 A standard network analysis, as currently implemented in the field, typically assesses a number of dif-
120 ferent topological measures in parallel, such as characteristic path length, average clustering, efficiency, and
121 small-world characteristic, among others (c.f., Rubinov and Sporns, 2011). Many of these characteristics,
122 however, are not independent of each other. In fact, they are often interrelated and can greatly influence
123 each other (van Wijk et al., 2010; Braun et al., 2012; Zalesky et al., 2012). Consider two metrics often
124 employed in graph theoretic analysis of brain data: clustering coefficient and density. Clustering coefficient
125 can be described as the level of segregated neural processing within a network (Rubinov and Sporns, 2010).
126 Density, as explained above, is a measure of the number of existing edges within a network (i.e., connection
127 with non-zero value), divided by the total number of possible edges. These two network characteristics are
128 strongly interrelated: It has been shown that there is a clear relationship between a network's density and its
129 clustering coefficient (Zalesky et al., 2012). Similarly, dependencies between many other network measures
130 frequently employed in the neuroimaging literature (e.g., degree, clustering coefficient, characteristic
131 path length, and small world index) have also been reported (van Wijk et al., 2010; Braun et al., 2012),
132 highlighting the need to control for these relationships in order to minimize the potential for spurious
133 findings (see Rubinov and Sporns, 2010; van Wijk et al., 2010). Conventionally, this problem is addressed
134 by arbitrarily fixing network density (see Problem #1). This approach, however, suffers from two important
135 shortcomings. First, as explained above, different networks might well have different levels of natural – or
136 stable – density. Second, it is a rather weak control. For, it only addresses the dependencies of network
137 measures on density, but ignores the many other known correlations among features of networks that are
138 often assessed (cf., van Wijk et al., 2010), which, to date, have gone unaccounted for in virtually all of the
139 extant literature in the field.

140 1.1.3 Problem #3: Failure to account for structural information in shaping functional networks

141 In the clinical context of DOC, despite the fact that patients are well known to have heterogeneous
142 underlying pathology, which introduces many concerns for proper diagnosis (Bruno et al., 2011; Coleman
143 et al., 2009), functional (e.g., Boly et al., 2012b; Crone et al., 2017a,b; Ku et al., 2011; Lee et al., 2009;
144 Laureys et al., 2000b; Monti et al., 2013; Rosanova et al., 2012) and structural connectivity (Fernández-
145 Espejo et al., 2011, 2012; Newcombe et al., 2010; Wilson, 2010; Tollard et al., 2009; Zheng et al., 2017)
146 are typically investigated separately. This narrow approach is very problematic because it has been shown,
147 in the rodent model (Díaz-Parra et al., 2017) and in healthy humans (Bettinardi et al., 2017; Messé et al.,
148 2015), that structural data can predict the functional connectivity as estimated by correlations in the fMRI
149 signal, as well as EEG phase coupling in healthy volunteers (Finger et al., 2016). Failing to include both

150 structural and functional data will have a similar effect on the analysis of functional networks as omitting
151 any other graph metric (i.e., problem #2): it will result in improper estimation of the terms in the model
152 and potentially spurious results. This issue is particularly important in the clinical context of DOC given
153 their highly heterogeneous pathology and the fact that this can change over time, which affects longitudinal
154 comparison of brain networks over time.

155 Diffusion weighted imaging (DWI) and blood oxygenation level dependent (BOLD) can be used in
156 conjunction to estimate connectivity matrices using joint independent component analysis (jICA; [Kessler
et al., 2014](#)), Connectivity Independent Component Analysis (connICA; [Amico and Goñi, 2017](#)) or partial
157 least squares (PLS; [Mišić et al., 2016](#)). In general, all three methods produce multiple group connectivity
158 matrices based on the covariance of BOLD and DWI data across all participants. Both jICA and connICA
159 produce multiple components that are maximally spatially independent (for a complete explanation of
160 jICA see [Calhoun et al., 2006, 2009; Sui et al., 2011](#), and for a complete explanation of connICA see
161 [Amico et al., 2017](#)). PLS produce a linear combination of latent variables that maximally covary with
162 each other based on weighted structural and functional connections (for a complete explanation of PLS
163 see [McIntosh and Lobaugh, 2004; Abdi, 2010; Krishnan et al., 2011; McIntosh and Mišić, 2013](#)). These
164 methods incorporate both structural and functional connectivity in the estimation of the connectivity
165 matrices, but they require researchers to choose the number of components (in jICA and connICA) or
166 number of latent variables (in PLS). Changing these parameters influences the results of the connectivity
167 estimation and the standards for these parameters are still being investigated for both jICA and connICA
168 ([Hyvärinen and Oja, 2000; Calhoun et al., 2009; Abou-Elseoud et al., 2010; Ray et al., 2013](#)). We thus
169 propose an alternative to these methods that avoids the necessity to estimate the functional and structural
170 connectivity jointly. In the approach we describe below, the structural and functional connectivity matrices
171 are estimated separately, and the former is used as a variable in estimating graph statistics for the latter (see
172 section §2.6 for a complete description).

174 1.1.4 Problem #4: Network dynamics – Estimating network change over time

175 Finally, contrary to the assumption underlying conventional network analysis in neuroimaging,
176 connectivity between areas is unlikely to be stationary processes. Rather, brain activity might best be
177 viewed as a malleable and variable process over time ([Ioannides, 2007](#)). Yet, even in the few cases where
178 this limitation has been addressed (e.g., [Barttfeld et al., 2015](#)), these types of approaches do not quantify
179 dynamic change of connectivity across time (or states). Rather, they just dissect a time-series into multiple
180 static networks and compare them over their respective topological properties. In other words, even these
181 approaches are static in nature and fail to capture the dynamics of network connectivity over time. In the
182 context of DOC, for example, this means that longitudinal analysis of brain data can be employed to reveal
183 differences in topological properties of networks at two different time-points, but do not allow saying
184 anything of the process of interest, which is the dynamics of how one network transitioned into another
185 (e.g., how a network transformed as consciousness was regained over time).

186 1.2 Exponential Random Graph Models (ERGM)

187 In response to these four shortcomings of current network analysis, we present and demonstrate a
188 novel (in the context of DOC, for other contexts within neuroimaging, cf.: [Simpson et al., 2011, 2012,
189 2013](#)) approach to graph analysis, referred to as Exponential Random Graph Models (ERGM; [Holland
and Leinhardt, 1981](#)). The core idea underlying ERGM is that instead of considering graphs as fixed
190 entities which can be described in terms of topological properties (e.g., clustering, path length, small world
191 property), it attempts to generate hypotheses about the (unobserved) stochastic processes that gave rise to
192

193 an observed network (Robins et al., 2007). Contrary to the prevalent approach in neuroimaging, then, the
 194 presence/absence of an edge within a network is not considered to be a fixed property of a graph, but rather
 195 a random variable generated by a stochastic process. In other words, rather than assuming the observed
 196 network as “given” and fix, and describing its topological characteristics (e.g., characteristic path length,
 197 clustering coefficient), it tries to characterize the processes that have generated the observed network. One
 198 particularly appealing aspect of this approach is that, so long as the total number of nodes (i.e., ROIs)
 199 constituting a network remains unchanged, it allows for comparing across networks with different density
 200 levels, thereby solving problem #1. The ERGM framework uses the following exponential model:

$$P_{\theta}(Y = y) = \frac{\exp(\theta^T g(y))}{c(\theta)} \quad (1)$$

201 where θ is a parameter vector that is modeled by $g(y)$ (i.e., any statistic of the graph). The parameter
 202 $c(\theta)$ is a normalizing constant representing the parameter estimate for all possible graphs (Hunter et al.,
 203 2008). This normalizing constant is not able to be analytically solved due to the combinatorics of the graph
 204 structure. We can nonetheless approximate the unknown population mean using $c(\theta_s)$ (i.e., the sample
 205 mean):

$$\begin{aligned} \frac{c(\theta)}{c(\theta_s)} &= E_{\theta_s} \exp(\theta - \theta_s)^T g(y_i) \\ \frac{c(\theta)}{c(\theta_s)} &\approx \frac{1}{M} \sum_{i=1}^M \exp(\theta - \theta_s)^T g(y_i) \end{aligned} \quad (2)$$

206 for derivations (see Hunter et al., 2008). These equations allows for an approximation of the population
 207 mean using sample mean. A bootstrapping method using Markov Chain Monte Carlo (MCMC) methods
 208 is used to sample and estimate the population mean. These methods assume Markovian principles of
 209 independent draws and the ability to reach equilibrium. Equilibrium is the state in which any edge that
 210 is toggled on or off results in an equally probable graph. The general method is to take the ratio of the
 211 probabilities of $Y_{ij} = 1$ (i.e., adding a single edge) and $Y_{ij} = 0$ (i.e., no edge) conditioned on $Y_{ij}^C = y_{ij}^C$
 212 (i.e., all other pair of nodes in the graph).

$$\begin{aligned} \frac{P(Y_{ij} = 1 | Y_{ij}^C = y_{ij}^C)}{P(Y_{ij} = 0 | Y_{ij}^C = y_{ij}^C)} &= \exp \theta^* (s(Y_{ij} = 1) - s(Y_{ij} = 0)) \\ \log \frac{P(Y_{ij} = 1 | Y_{ij}^C = y_{ij}^C)}{P(Y_{ij} = 0 | Y_{ij}^C = y_{ij}^C)} &= \theta^* \Delta(s(Y_{ij})) \\ \text{LPL}(\theta) &= \sum \log [P(Y_{ij} = y_{ij}) | (Y_{ij}^C = y_{ij}^C)] \end{aligned} \quad (3)$$

213 where the $\text{LPL}(\theta)$ is the log-pseudolikelihood for θ , which is maximized by taking the maximum pseu-
 214 dolikelihood for θ (Hunter et al., 2008). This estimation process is performed for the model with all the
 215 parameters (i.e., θ). The estimates give the mean and standard error. These estimates were tested for
 216 significance in each functional data set. Due to the MCMC, a t-statistic can be estimated and is reported in
 217 the model output along with a p-value.

218 For interpretation purposes, equation 1 can be represented as follows (the full derivations can be found
219 in Hunter et al., 2008):

$$\text{logit}(P_{\theta}(Y_{ij} = 1 | n_{actors}, Y_{ij}^C)) = \sum_{k=1}^K \theta_k \delta_{Z_k(y)} \quad (4)$$

220 where k is the number of network statistics in the model and θ_k is the parameter estimate for each statistic.
221 The $\delta_{Z_k(y)}$ is the change in network statistic if a edge were added between any node i and j . Thus, the
222 interpretation of the network statistics involve the change in probability of an adding a edge with certain
223 network statistic. The significance of a parameter estimate is one compared to the expected parameter
224 estimate in a null model with the probability of all edges equal to 0.5 (i.e., Erdős and Rényi, 1959).

225 In what follows, we first demonstrate the insidiousness of problem #2 in the context of well characte-
226 rized, freely-available, data on the business ties of Florentine families in the 15th century (Kent, 1978), and
227 then we apply the powerful and flexible ERGM approach to estimating network statistics for characterizing
228 (brain) networks in the longitudinal context of a patient recovering after coma after severe traumatic brain
229 injury (TBI). To anticipate the key points that will follow, ERGM, which has been successfully employed
230 in other contexts (Goodreau et al., 2009; Handcock et al., 2017; Holland and Leinhardt, 1981; Hunter,
231 2007; Hunter et al., 2008), offers a number of substantial advantages which are particularly important in
232 the clinical context of DOC. First, it does not require imposing (and assuming) the same level of density
233 across graphs, thus allowing estimating characteristics of each graph at its “natural” density level. Second,
234 it allows for controlling the dependencies between network characteristics. In this sense, in contrast to
235 the conventional approach, which can be viewed as a series of univariate regressions (i.e., one per metric)
236 assessing the topological characteristics across groups of graphs (e.g., patient groups, controls versus
237 patients, etc), ERGM is making use of a multiple regression framework (Goodreau et al., 2009), in which
238 all features are considered together, and thus returns the “unique” contribution of each network measure.
239 Third, the multiple regression framework extends to graph theoretic measures characterizing the structural
240 connectivity of a network, thus accounting and “parceling out” the effect of cross-sectional differences
241 (e.g., Zheng et al., 2017) and longitudinal changes in structural connectivity (e.g., Voss et al., 2006;
242 Thengone et al., 2016) across graphs. Finally, a temporal implementation of this technique, Separable
243 Temporal ERGM (STERGM), allows assessing the dynamic changes of network properties occurring over
244 observations (e.g., time, clinical groups).

2 METHODS

2.1 Florentine Business Ties Data

246 We demonstrate the importance of problem #2 using freely available data for social network analysis.
247 The dataset, which has been extensively characterized in previous work, describes business connections
248 between Florentine families in the 15th century (Kent, 1978). We use this data analysis to demonstrate
249 the interrelationship between network measures and how failure to include them in a single full model
250 can lead to spurious results. Specifically, the relationship between network measures is manipulated
251 by constructing two identical networks with one unique difference between them – that is, whether the
252 Barbadori family belongs to the blue group (Figure 1, left) or the green group (Figure 1, right). As we will
253 discuss further below, this example focuses on the relationship between node mixing terms (i.e., a measure
254 of within-group [blue versus green] connectivity) and a higher order term called geometrically weighted
255 edge shared partners (GWESP; a type of triangles term; see section §2.6 for full description of both terms).

256 To demonstrate the effects of relationships between measures, we estimate three models per each network:
 257 two partial models including an edges term and either the higher order term (PM_A) or the mixing terms
 258 (PM_B), and the Full model (FM) containing all terms. As we will show, for each network, partial models
 259 return spurious results with respect to both significance and magnitude of the parameter estimates.

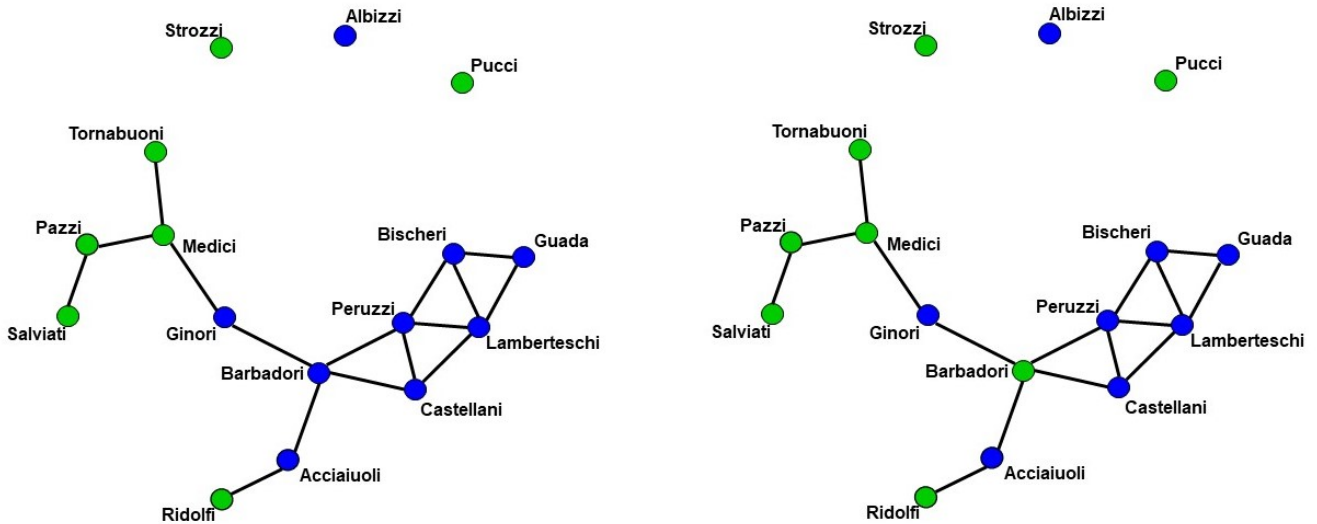


Figure 1. Florentine business ties networks. Florentine business ties data with additional grouping. Left: Network A. Right: Network B. We note that two networks are identical except for the Barbadori family being allocated to the blue group in the left graph and to the green group in the right graph.

260 2.2 Patient

261 We demonstrate the use of ERGM models using longitudinal data from a patient recovering from a
 262 severe brain injury. A 40 to 45 year old person suffered a severe TBI due to a fall. The patient suffered
 263 pulmonary contusion and liver laceration, and presented with a post-resuscitation Glasgow Coma Scale
 264 (GCS; [Teasdale and Jennett, 1974](#)) of 3. Computerized tomography (CT) revealed skull fractures, traumatic
 265 subarachnoid hemorrhage, extradural hematoma, subdural hematoma, and bilateral frontal lobe contusions.

266 2.3 Experimental Design

267 The patient underwent 4 imaging sessions over the span of 6 months post injury. The first 3 sessions
 268 occurred within a month post injury on the 11th, 18th and 25th days post-injury. The chronic session
 269 took place 181 days post-injury. At the time of the acute imaging sessions, the patient presented a GCS
 270 of 3, 6, and 10, respectively. At each session the patient underwent (among other clinical and research
 271 sequences) anatomical (T1-weighted) and functional (T2*-weighted) data protocols. T1-weighted images
 272 were acquired with a 3D MPRAGE sequence (repetition time [TR] = 1900 ms, echo time [TE] = 3.43,
 273 $1 \times 1 \times 1$ mm). BOLD functional data were acquired with a gradient-echo echo planar image (TR = 2000
 274 ms; TE = 25 ms, $3.5 \times 3.5 \times 4$ mm). Diffusion Weighted data were acquired with an echo planar sequence
 275 (TR = 9000 ms, TE = 90 ms, 64 directions, $3 \times 3 \times 3$) using a b-value of 1000 and acquiring an additional
 276 B0 image. Data were acquired on a 3 Tesla Siemens TimTrio and a 3 Tesla Siemens Prisma system at the
 277 Ronald Reagan Medical Center at the University of California Los Angeles. The study was approved by
 278 the UCLA institutional review board (IRB). Informed consent was obtained from surrogates, as per state
 279 regulations.

280 2.4 Data Preprocessing

281 2.4.1 BOLD data preprocessing

282 The functional data underwent a number of conventional preprocessing steps including brain extraction,
283 slice timing correction, motion correction, band-pass filtering ($0.08 \leq \text{Hz} \leq 0.1$), and removal of linear
284 and quadratic trends. A nuisance regression was employed to parcel out signals of non-interest including
285 motion parameters, white matter, cerebral spinal fluid, and full-brain mean signal (which has been shown to
286 alleviate the consequences of in-scanner motion; Power et al., 2012). Affine registration of the functional
287 data to the standard template (MNI) was performed using Advanced Normalization Tools (ANTs; Avants
288 et al., 2008, 2011).

289 2.4.2 DWI data preprocessing

290 The diffusion data were preprocessed using the following pipeline: DWI preprocessing, registrations,
291 probabilistic tractography with tractography thresholding. All of these processes were run using a bash
292 script in parallel using the GNU Parallel package (Tange, 2011).

293 **DWI preprocessing.** All preprocessing procedures were visually checked for optimal quality. The T1-
294 weighted data were brain extracted (optiBET; Lutkenhoff et al., 2014) and bias field corrected (BrainSuite
295 BFC; Shattuck et al., 2001). The diffusion-weighted data were prepared for tractography with the following
296 steps: 1) visual quality checking of raw images; 2) artifact checking/removal and motion correction with
297 vector rotation (DTIprep; Oguz et al., 2014); 3) eddy current distortion correction followed by tensor
298 fitting and estimation of diffusivity metrics (BrainSuite's BDP; Bhushan et al., 2012; Haldar and Leahy,
299 2013); 4) brain extraction of the b0 image (BET; Smith, 2002); and 5) GPU-enhanced Bayesian estimation
300 of the diffusion profile with up to two principal directions per voxel (i.e., allowing for crossing/kissing
301 streamlines) using FSL's bedpostx (Behrens et al., 2003; Hernández et al., 2013).

302 **Registrations.** All registrations were visually checked for optimal quality. The following steps were
303 conducted: 1) linear registration of the native diffusion data (b0 image) to the native T1-weighted data
304 (ANTs' IntermodalityIntrasubject; Avants et al., 2011); 2) nonlinear registration (ANTs) of the native
305 T1-weighted data to the Montreal Neurological Institute (MNI) standard space (MNI Avg 152 T1 2x2x2mm
306 standard brain); 3) forward or inverse transform concatenations (ANTs; Avants et al., 2011) to move
307 between native diffusion, native T1, and the MNI template.

308 **Probabilistic tractography.** GPU-enhanced probabilistic tractography between all regions of the
309 whole-brain atlas (i.e., iteratively seeding from each region to all other regions as targets) was conducted
310 with the "matrix1" option in FSL's probtrackx2 (Behrens et al., 2003, 2007). A minimum distance of
311 4.8mm (i.e., 2 voxel widths) was set to prevent artificial streamlines passing through contiguous regions.
312 The output matrix of streamline counts between all regions was thresholded to remove spurious streamlines
313 with an optimization procedure that minimizes asymmetries between the seed/target assignments for each
314 ROI-ROI pair (MANIA; Shadi et al., 2016).

315 2.5 Brain Network Construction

316 For each dataset (both the functional and diffusion data), a graph was constructed to provide a
317 mathematical description of the brain as a functional network. Brain graphs were constructed in two steps.
318 First, these data sets were parceled into 148 ROIs spanning the cortex, sub-cortical nuclei, cerebellum and
319 brainstem (see Figure 2). This parcellation scheme, which was defined independently of our data, is made
320 freely available by Craddock and colleagues (Craddock et al., 2012). While other parcellation schemes are

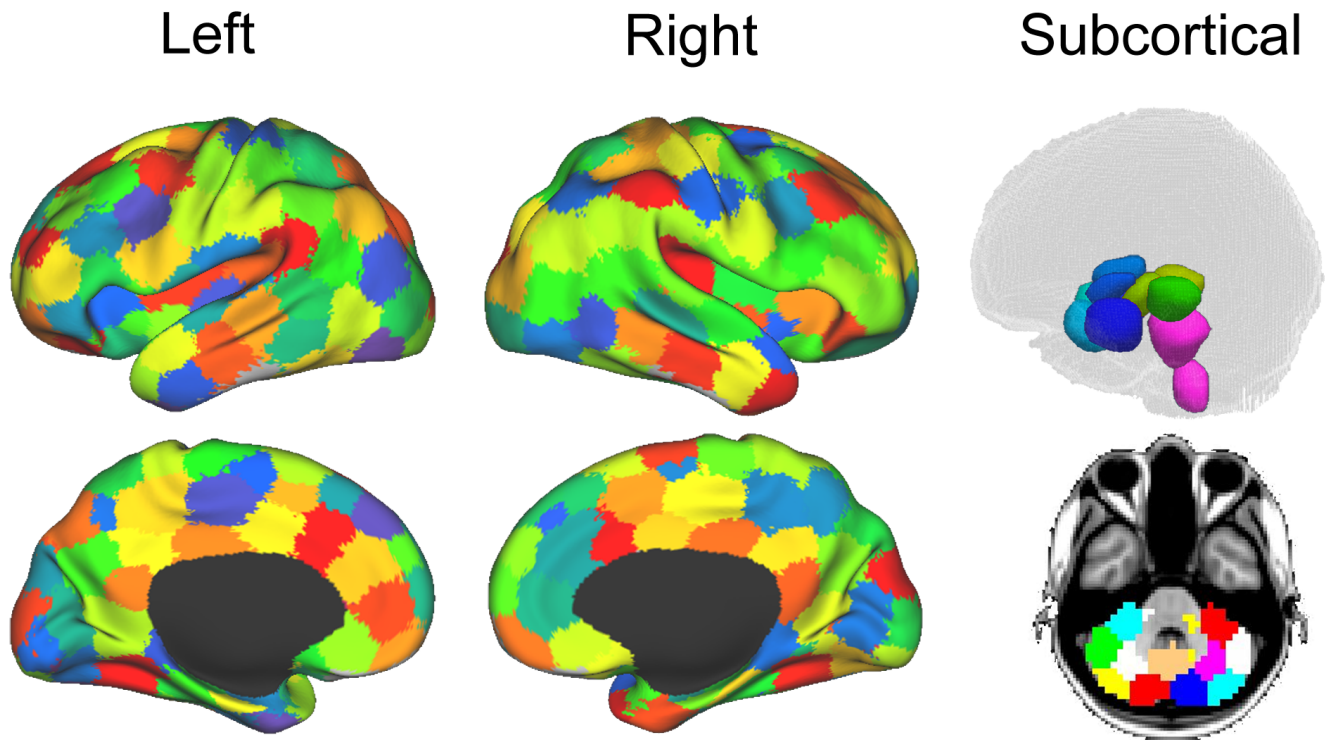


Figure 2. Parcellation for structural and functional connectivity. Cortical and subcortical parcellation of the brain data (Craddock et al., 2012). The imaging sessions' data sets were parcellated into 148 ROIs throughout the cortex, sub-cortical nuclei, cerebellum and brainstem. (Figure from Monti et al., 2013)

321 available (e.g., Harvard-Oxford atlas, AAL atlas), the present one has two main advantages (cf., Monti
 322 et al., 2013). First, being functionally defined, it clusters spatially proximal voxels by the homogeneity of
 323 their functional connections as opposed to clustering voxels by anatomical position which, as exemplified
 324 by the case of the precentral gyrus ROIs in both the AAL and the Harvard-Oxford atlases, might cluster
 325 together functionally distinct sub-regions. Second, at our chosen level of resolution, the Craddock ROIs
 326 have almost twice the granularity as either structural atlas (i.e., 193 ROIs versus, 90 and 112 for the AAL
 327 and Harvard-Oxford atlases, respectively). Following parcellation, the average time-course of all voxel
 328 within each ROI were extracted and correlated across each pair of regions.

329 Functional connectivity was assessed with a partial correlation method using the Markov Network
 330 Toolbox (MoNeT; Narayan et al., 2015) in MATLAB. This approach, referred to as R3 (as in resampling,
 331 random penalization, and random effects), combines a penalized maximum likelihood estimation – or
 332 graphical lasso – procedure with a resampling-based (bootstrapped) model selection procedure, on whitened
 333 BOLD timeseries, to infer fully-data driven stable functional connectivity estimates at the single-subject
 334 (or group) level. Under this approach, each fMRI time series is repeatedly bootstrapped in order to
 335 estimate the within-subject variability and matrices of penalty parameters which reduce selection bias and
 336 variability. This method thus reduces the spurious connections from indirect sources arising from the high
 337 dimensionality of fMRI data often seen when using the conventional Pearson's r method. Using partial
 338 correlations with regularization parameters, the indirect sources are eliminated and the sparsity of each
 339 matrix is determined by the within subject variability. Thus, each functional data set returns a connectivity
 340 matrix that represents connectivity from direct sources, rather than indirect ones, and that is sparse, as
 341 determined on a single-subject basis through bootstrapping and regularization. This latter point side-steps

entirely the need for arbitrary and iterative thresholding approaches (Rubinov and Sporns, 2010). It is important to point out, however, another important difference between the partial correlations approach described above and the standard correlation approach to estimating brain networks as performed by most previous work (e.g., Boveroux et al., 2010; Monti et al., 2013; Schrouff et al., 2011). On the one hand, the conventional correlational approach has the advantage of allowing straightforward interpretation of the elements of adjacency matrices as strength of the functional connectivity between nodes. On the other hand, the matrices generated are fully connected and thus requiring application of a non-linear transformation (e.g., thresholding) in order to render them sparse – a condition necessary for application of many common graph theory metrics (Rubinov and Sporns, 2010). In contrast, the partial correlation method employed here returns a sparse matrix. However, it does so at the cost of losing interpretability of graph weights which can now be seen as the functional connectivity between two nodes i and j after controlling for the correlations with other nodes in the neighborhood (i.e., connected with) – say – i . For this reason, matrices obtained with this novel methodology are typically binarized, thus resulting in a sparse matrix of ones and zeros indexing the presence/absence of functional connectivity between each pair of nodes (i.e., ROIs).

2.6 Graph Statistics

All ERGM models we used to analyze the patient data included the same graph statistics. The model used for all the data sets was specified as follows:

$$P_{\theta}(Y = y) = \frac{\exp(\theta_1 \text{edges} + \theta_2 \text{nodecov}(\text{degree}) + \theta_3 \text{nodecov}(\text{efficiency}) + \theta_4 \text{nodecov}(\text{cluster}) + \theta_5 \text{nodemix}(\text{latent}) + \theta_6 \text{nodemix}(\text{resting}) + \theta_7 \text{gwesp}(\alpha = \lambda))}{c(\theta)} \quad (5)$$

Edges refers to the total number of edges for each functional connectivity graph. This term allows control for the density of each graph. In this sense it is thus similar to the intercept in a linear regression and is thus typically not interpreted or further analyzed.

There are four nodal covariate terms for the diffusion data—three nodal covariates (i.e., degree, efficiency and cluster) and the nodemix (latent) term –and a nodal covariate for the functional connectivity (i.e., nodemix for resting). Degree is the number of edges for each structural node. Efficiency is the local efficiency of each node. Cluster is the clustering coefficient of each node. The nodecov term estimates the probability of functional connectivity edge as a function of each distribution of the structural terms (i.e., degree, local efficiency and clustering coefficient). A positive coefficient indicates an increase in the probability of a functional connectivity edge as structural term increases in magnitude. On the other hand, a negative coefficient indicates an increase in probability of a functional connectivity edge as the structural term decreases.

As shown in equation 5, there are two nodemix terms: latent and resting. The nodemix (latent) is the within and between module connectivity of the structural connectivity. Thus, this mixing term represents the probability of a functional connectivity edge given the modular membership based on the structural connectivity. The number of modules and modular membership of each node is determined by a position latent cluster ERGM (Handcock et al., 2007; Krivitsky and Handcock, 2008). These models have shown to be able to use a latent space model with an a priori determined number of dimensions using the parameter d (3 dimensions). The nodes are arranged in a euclidean system with proximity equating to probability of an edge. The clusters are determined by the parameter G (3, 4, 7 and 6 for Acute first, second, third sessions and Chronic session, respectively). This parameter sets the number of Gaussian spherical clusters that

380 are introduced in the latent space. The estimation of position latent cluster ERGM is a two step Bayesian
 381 estimation, but the exact specification is beyond the scope of this paper (see [Handcock et al., 2007](#)).

382 The nodemix (resting) is our mixing term for determining the inter- and intra-regional connectivity of
 383 the resting state networks and sub-cortical regions of the functional data. Multiple parameter estimates were
 384 produced for this term. Additionally, these mixing terms used the exogenous node labels for each node's
 385 membership in the seven resting state networks ([Yeo et al., 2011](#)) and sub-cortical regions. Each node of
 386 the brain network was labeled either: frontoparietal, visual, somato-motor, limbic, dorsal attention, ventral
 387 attention, default, subcortex and thalamus. Each combination of the inter- and intra-regional connectivity
 388 produced a mixing term and parameter estimate. For example, one inter-regional mixing term would be
 389 frontoparietal and thalamic connectivity. This parameter estimate would give the probability of an edge
 390 existing between the frontoparietal network and thalamus. An example of intra-regional mixing term
 391 would be frontoparietal to frontoparietal. This term would express the probability of an edge within the
 392 frontoparietal network. These mixing terms were used to assess the connectivity between the within the
 393 resting state networks, between the resting state networks, within the sub-cortical regions, between the
 394 sub-cortical regions, and between resting state networks and sub-cortical regions. This term incorporates
 395 questions that would be addressed using seed based connectivity analyses.

396 The geometrically weighted edged shared partners (GWESP) can be expressed by this equation
 397 ([Hunter, 2007](#)):

$$\begin{aligned}\theta_t &= \log \lambda_t \\ v(y; \theta_t) &= e^{\theta_t} \sum_{i=1}^{n-2} \left[1 - (1 - e^{-\theta_t})^i \right] EP_i(y)\end{aligned}\quad (6)$$

398 In this equation, v is the GWESP term and θ_t is the log of the decay parameter that was fixed in
 399 all the data sets. The $EP_i(y)$ is the edge shared partners term for the entire graph. It accounts for the
 400 number of each type of edge shared partner. An edged shared partner is triangle that shares a common base.
 401 Edge shared partners is a metric used to quantify the amount of clustering in the form of transitivity in a
 402 network. High positive parameter estimates indicate that transitivity is present above and beyond all the
 403 other statistics in the model. Transitivity is a higher order relationship present in most graphs which are the
 404 local and/or global communication and the amount of local cohesion. Differences in transitivity between
 405 patients could be a key change that occurs from injury. This would be a disruption of the clustering found
 406 within the patient's brain. This type of disruption would hamper local and/or global communication and
 407 additionally it would indicate a lack of local cohesion within a network.

408 The analysis was performed using the ERGM package ([Handcock et al., 2017](#)) in R. There are two
 409 ERGMs used on the patient data. A full model (FM) and used all the terms from equation 5. The FM
 410 was fit multiple times to get assess the proper λ (the decay parameter) for the GWESP term. The range of
 411 λ began at 0.05 and increase by increments of 0.05 up to 2.0. Each iteration was checked by inspecting
 412 the diagnostics of the MCMC. The models that have the best fit for the parameter estimate GWESP were
 413 chosen (i.e., $\lambda = 0.45$). A second model, the partial model (PM) was fit. The structural terms (i.e., the three
 414 nodecov and the nodemix for latent) were omitted from this model to demonstrate the effects on the rest of
 415 the parameter estimates.

416 The FM's graph statistics were chosen based on two reasons: the type of functional data being
 417 analyzed (i.e., resting state data) and the first three problems outlined above (see section §1.1.1, §1.1.2 and

418 §1.1.3). The nodemix (resting) terms were chosen because this patient's functional connectivity matrices
419 were estimated from the BOLD correlations during the resting state scans. Thus, the intra- and inter-
420 regional connectivity would be best characterized by putative resting state networks. The number of resting
421 networks were chosen based on a data driven approach (i.e., Yeo et al., 2011) that estimates a number
422 of networks based on stability of clusters (for details on the clustering algorithm see Lashkari et al.,
423 2010) estimated from 1000 subjects' functional data. A seven network parcellation was chosen because it
424 minimized the instability (Yeo et al., 2011) and matches what has been previously discussed in the literature
425 (e.g., Buckner, 2010; Cohen et al., 2008; Fox et al., 2006; Vincent et al., 2008). Additionally, the thalamus
426 group was added because of its possible involvement in DOC (e.g., Crone et al., 2014; Laureys et al.,
427 2000b; Vanhaudenhuyse et al., 2010; Zhou et al., 2011) or anesthesia induced loss of consciousness (e.g.,
428 Boveroux et al., 2010; Martuzzi et al., 2010; Schrouff et al., 2011; Stamatakis et al., 2010). Finally, the
429 subcortical and cerebellum groups were added to ensure every node fit a grouping label.

430 The edges term allows for networks with varying density to be modeled and compared (cf., Problem
431 #1, section §1.1.1). The higher order term (i.e., GWESP) describes the local and/or global communication
432 which could be an important aspect in the recovery from brain injury (e.g., Chennu et al., 2014; Crone
433 et al., 2014; Schröter et al., 2012), and because it alleviates the problem of interrelation among graph
434 theoretic measures (cf., Problem #2, section §1.1.2) by accounting for the higher order term's variance and
435 thus avoiding it being improperly allocated to lower order terms (i.e., edges, node mixing, and structural
436 terms). As shown below, failing to include the higher order term can affect the estimation of parameters
437 in either magnitude or sign. Structural connectivity is important because, as stated in third problem (cf.,
438 section §1.1.3), it can be severely affected by TBI, systematically changing over time and/or patient cohorts,
439 and because it is interrelated with functional connectivity. Thus, we chose four terms for the structural
440 connectivity that would capture the number of connections of each node (i.e., degree), a measure of
441 integration (i.e., local efficiency Rubinov and Sporns, 2010), and higher order relationships (i.e., clustering
442 and modularity). The two higher order terms were chosen because they capture two different higher order
443 dynamics: local grouping of nodes (i.e., clustering coefficient Rubinov and Sporns, 2010) and community
444 structure (i.e., modularity; Rubinov and Sporns, 2010). Overall, our model controls for the density of
445 the functional connectivity and the effects of structural connectivity on the functional connectivity while
446 modeling the intra- and inter-connectivity of the resting state networks and the effects of higher order terms
447 (i.e., GWESP).

448 The models were assessed by using goodness of fit (GOF) plots (Hunter et al., 2008). After the model
449 was estimated, a thousand simulations were run from the model statistics. These simulations were compared
450 to the original graph's probabilities for each graph statistic (e.g., the probability of nodes with a specific
451 degree, probability edge shared partners and the probability minimum geodesic distances). This is to ensure
452 that the model represents a graph similar to the original data that it was modeled from. The metrics chosen
453 for this example is degree distribution, edge wise shared partner, minimum geodesic distance (another form
454 of local path length) and the nodal covariates from equation 5. These are the most commonly used graph
455 metrics because they capture important characteristics of graphs that capture the central tendencies and
456 clustering of graphs. The MCMC diagnostics were assessed for each parameter estimate. The GOF plots
457 were used to assess the fit of the FM and all four GOF plots was assessed for goodness of fit.

458 2.7 Separable Temporal Exponential Random Graph Model

459 STERGM (Krivitsky and Handcock, 2014) is an extension of the original ERGM. It is used to assess
460 the dynamics of networks as they change over time. The same underlying methods for estimating ERGM

461 is used in STERGM. A model with network statistics is used to estimate the parameter estimates for a
 462 network that changes over time. To achieve this, two separate networks are investigated. A formation
 463 network is generated conditional on forming edges,

$$P(Y^+ = y^+ | Y^t; \theta^+) = \frac{\exp(\theta^+ g(y^+, X))}{c(\theta^+, X, Y^+(Y^t))}, y^+ \in Y^+(y^t) \quad (7)$$

464 where a formation network Y^+ is characterized by formation parameters θ^+ (Krivitsky and Handcock,
 465 2014). The formation network statistics are $g(y^+, X)$ and the normalizing constant is $c(\theta^+, X, Y^+(Y^t))$.
 466 The second network formed is a dissolution network that is conditional on the edges that dissolve. This
 467 network is represented by the same variables labeled with minus instead of a plus,

$$P(Y^- = y^- | Y^t; \theta^-) = \frac{\exp(\theta^- g(y^-, X))}{c(\theta^-, X, Y^-(Y^t))}, y^- \in Y^-(y^t) \quad (8)$$

468 where a dissolution network Y^- is characterized by dissolution parameters θ^- (Krivitsky and Handcock,
 469 2014). The dissolution network statistics are $g(y^-, X)$ and the normalizing constant is $c(\theta^-, X, Y^-(Y^t))$.
 470 These networks can form a new network at time $t + 1$ by applying formation and dissolution networks on
 471 y^t . This can be expressed as:

$$Y^{t+1} = Y^t \cup (Y^+ - Y^t) - (Y^t Y^-) \quad (9)$$

472 The formation and dissolution networks are independent of each other across the $t + 1$ time points
 473 (Krivitsky and Handcock, 2014). STERGM has the unique ability to model networks as they transform over
 474 time enabling research questions about the dynamics of a network. The same model in Equation 5 was used
 475 in both the formation and dissolution models. The quantifications of these networks are similar to ERGM,
 476 but these two models slightly change the interpretation of the parameter estimates. In the formation model,
 477 a positive parameter estimate indicates a tendency for edges for a network statistic form at time point $t + 1$,
 478 and a negative parameter estimate indicates a lack of formation of edges for a particular network statistic at
 479 time point $t + 1$. The dissolution model has two separate interpretations based on the sign of the parameter
 480 estimate. A negative parameter estimates are interpreted as edges are more likely to dissolve and positive
 481 parameters indicate edges are more likely to be preserved. Despite these differences in interpretation, all the
 482 same procedures were used in STERGM as were used in ERGM (PM, FM, quality control using MCMC
 483 diagnostics, and assessing fit using GOF) for both the formation and dissolution models.

3 RESULTS

484 3.1 Florentine Business Ties

485 Network A has both the mixing term and triangles term as significant model statistics when modeling
 486 them separately (i.e., PM_A and PM_B see Table 1). When they are combined together into the FM, the
 487 mixing term remains significant but the triangle term is no longer significant. Thus, the FM for the
 488 Florentine business ties properly attributes the variance of each graph theory statistic and the selective
 489 mixing term remains significant. The network B has just the triangles term significant in the PM_A and FM.
 490 The mixing term is neither significant in the PM_B nor the FM.

491 **3.2 Patient recovery**

492 Consistent with the argument we made in the introduction, as shown in Figure 3 (bottom row),
 493 the brain network construction using MoNeT resulted in four graphs with different estimated densities.
 494 Specifically, the three acute sessions returned graph densities of 10.4%, 13.5%, 12.9%, for the first, second,
 495 and third time-points, respectively, while the chronic session presented a graph density of 14.5%. Overall,
 496 then, the density differential between acute session 1 and chronic session was 4.1%, and the general
 497 acute-to-chronic pattern appeared to be a trend towards greater density. The structural connectivity (Figure
 498 3, top row), on the other hand, had less variability in the densities of the graphs over time (i.e., 6.6%, 6%,
 499 5.3% and 5.3%; a total difference of 1.3% between acute session 1 and chronic session).

500 **3.2.1 Integrating functional and structural connectivity**

501 When we compared the properties of the network as estimated relying exclusively on functional
 502 connectivity (i.e., partial model; PM) as compared to when both functional and structural connectivity
 503 were jointly considered (i.e., full model; FM), the PM included two significant positive inter-regional
 504 connectivity parameters (i.e., between thalamus and subcortex and between limbic network and subcortex;
 505 see top of Figure 4) which were no longer significant once structural connectivity was included (i.e., in the
 506 PM), suggesting their spurious status. More broadly, the positive parameter estimates became less positive
 507 and the negative parameter estimates became more negative. The only structural terms that were significant
 508 were the nodal covariate mixing term for connectivity between latent clusters 2 and 3 and within latent
 509 clusters 3 (see Table 2).

510 At the second acute time-point, the PM and the FM again differed, with the latter showing an additional
 511 significant positive parameter estimate for connections between dorsal attention network and subcortex
 512 (see bottom Figure 4), three inter-regional connectivity parameter estimates that became non-significant

	<i>ERGM Parameter Estimates</i>					
	<i>Network A</i>			<i>Network B</i>		
	PM_A	PM_B	FM	PM_A	PM_B	FM
Edges	-2.44*** (0.40)	-3.42*** (0.72)	-3.54*** (0.70)	-2.46*** (0.39)	-2.27*** (0.43)	-2.75*** (0.49)
Nodal Covariate Mixing: Within Group 0		1.63 (0.95)	1.60 (0.88)		0.15 (0.75)	0.31 (0.65)
Nodal Covariate Mixing: Within Group 1		2.60** (0.80)	2.16** (0.82)		1.17 (0.61)	0.91 (0.48)
GWESP (Fixed 0.8)	0.53* (0.23)		0.32 (0.28)	0.54* (0.23)		0.50* (0.23)

Note:

* $p < 0.05$; ** $p < 0.01$; *** $p < 0.001$

Table 1. Florentine business ties models. Three models are run on each network in figure 4: PM_A , PM_B , FM. The PM_A has just the edges and triangles term. The PM_B has just the edges and mixing term. The Full model has all three terms. Each term has a parameter estimate, a standard error in parenthesis and a p-value indicated by asterisks. The LATEX code to create this table was produced by the R package called texreg (Leifeld, 2013).

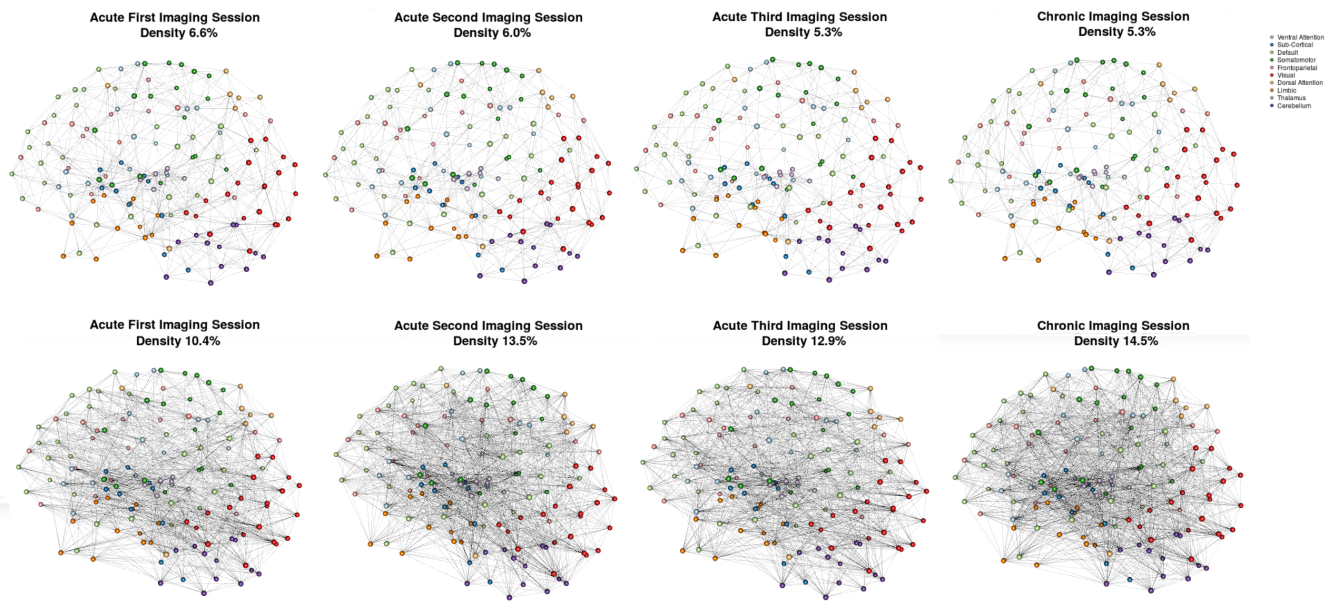


Figure 3. Patient recovery: Network densities. Top Four Graphs are the thresholded (MANIA; Shadi et al., 2016) structural connectivity. The first acute imaging session, second acute imaging session, third acute imaging session and chronic imaging sessions had 6.6%, 6%, 5.3% and 5.3% densities, respectively. Bottom Four Graphs are the thresholded functional connectivity using partial correlations (MoNeT; Narayan et al., 2015). The first acute imaging session, second acute imaging session, third acute imaging session and chronic imaging sessions had 10.4%, 13.5%, 12.9% and 14.5% densities, respectively.

513 (i.e., connections between cerebellum and subcortex, default network and frontoparietal network and visual
 514 network and dorsal attention; see bottom Figure 4) and two intra-regional connectivity parameter estimates
 515 that became non-significant (i.e., connections within the subcortex and ventral attention network; see
 516 bottom Figure 4). Overall, the parameter estimates both increased and decreased in magnitude with or
 517 without changing significance. Similar to the first acute session, the structural terms were only significant
 518 for the nodal covariate mixing term (i.e., between latent clusters 1 and 3, and within latent clusters 1, 2, 3
 519 and 4; see Table 2).

520 In the third acute session, six inter-regional positive parameter estimates (i.e., connections between
 521 cerebellum and dorsal attention network, frontoparietal network and dorsal attention network, frontal
 522 parietal network and ventral attention network, dorsal attention network and somatomotor network, limbic
 523 network and visual network and limbic network and subcortex; see right Figure 5) and three intra-regional
 524 positive parameter estimates (i.e., connections within the dorsal attention network, somatomotor network
 525 and ventral attention network; see Figure 5) became non-significant once structural connectivity was
 526 included in the model. Similar to the first acute session, the parameter estimates generally decreased in
 527 magnitude. Finally, consistent with the first two acute sessions, the only significant structural feature was
 528 the nodal covariate mixing term (i.e., between latent clusters 2 and 3, latent clusters 1 and 4, latent clusters
 529 1 and 6, latent clusters 3 and 6 and latent clusters 5 and 7, and within latent clusters 1, 2, 3, 4, 5, 6 and 7;
 530 see Table 3).

531 In the chronic session, two inter-regional positive parameter estimates became non-significant after
 532 inclusion of the structural connectivity terms (i.e., between default network and frontoparietal network
 533 and default network and visual network; see right Figure 5). Conversely, unlike in the acute sessions,
 534 we also observed the reverse effect, with the the visual network and ventral attention network parameter

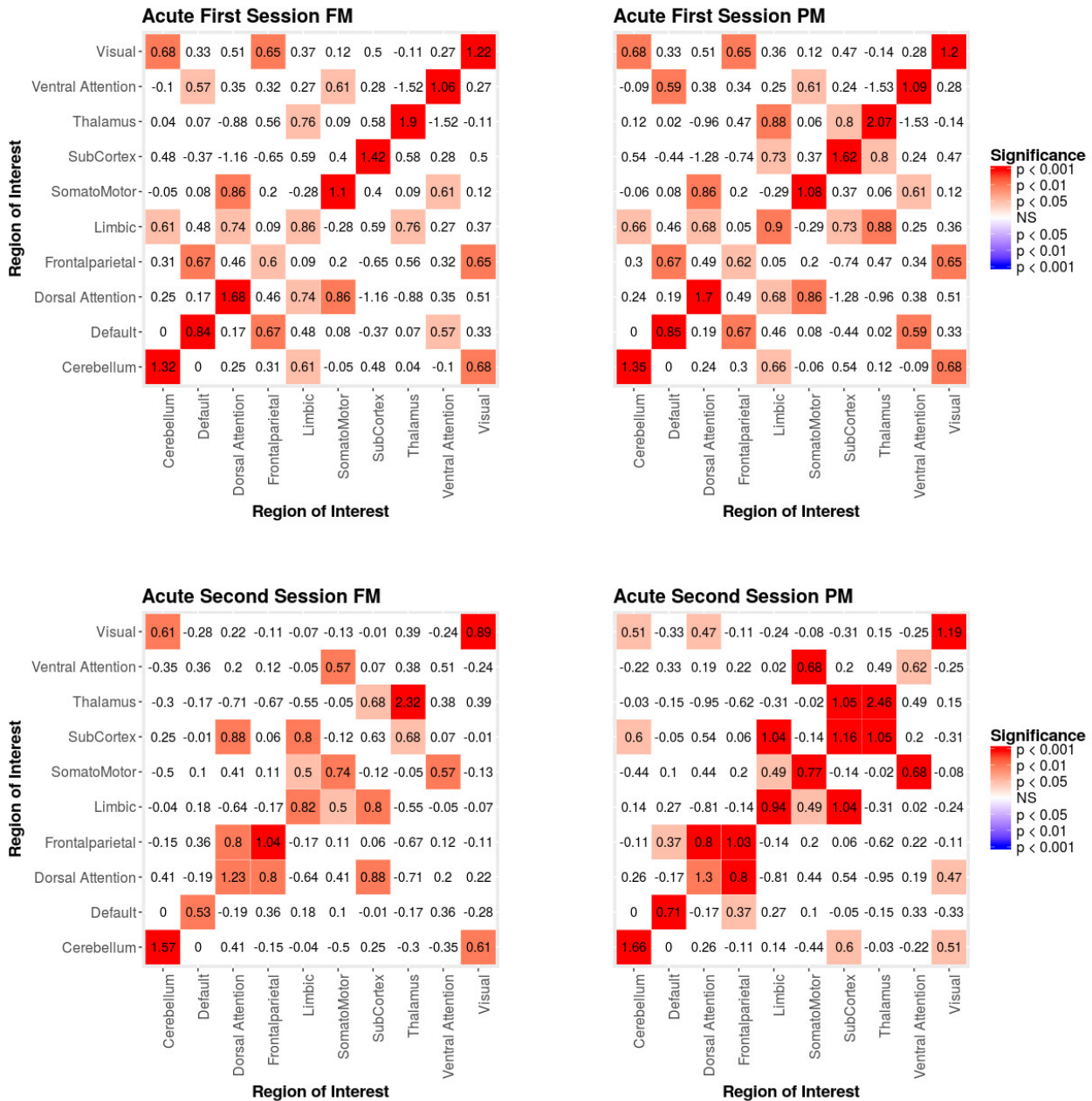


Figure 4. Patient recovery ERGM. Comparison of results for the FM and PM for acute sessions 1 and 2. The left figures display the FM mixing term results for the Acute first and second sessions. The mixing term accounts for the inter- and intra-regional connectivity. The legend displays tints of red for significant positive parameter estimates and the significant negative parameter estimates are colored in tints of blue. The right figures display the PM mixing term results for the Acute first and second sessions. The coloring scheme is the same as the FM. These figures are symmetric within each model because the graphs are undirected.

535 estimate became significant in the FM. Additionally, the structural terms were only significant for the nodal
 536 covariate mixing term (i.e., between latent clusters 1 and 3, latent clusters 2 and 3, latent clusters 1 and 4,
 537 latent clusters 3 and 5, latent clusters 4 and 5, latent clusters 1 and 6 and latent clusters 2 and 6 and within
 538 latent clusters 4; see Table 3).

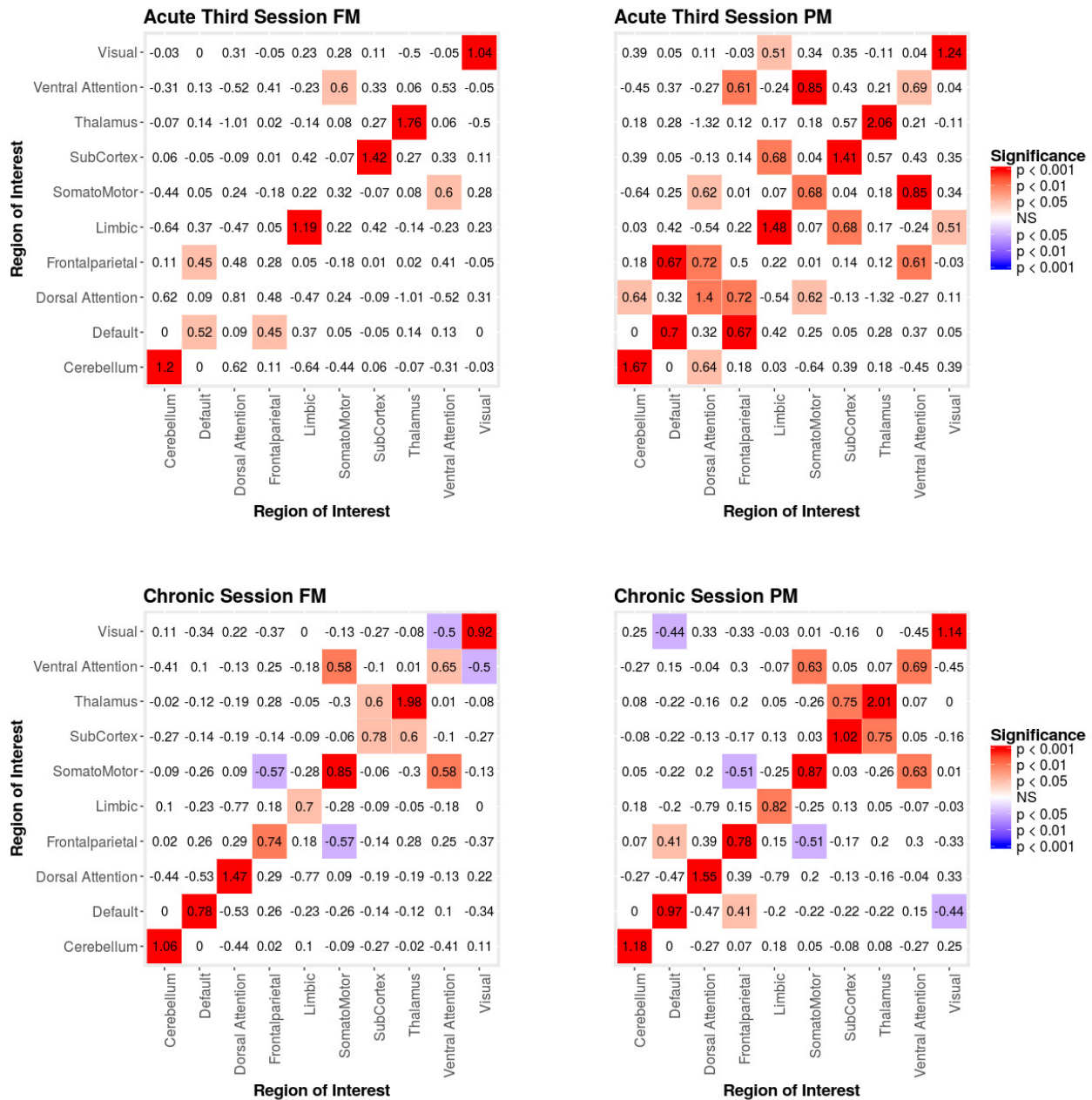


Figure 5. Patient recovery ERGM. Comparison of results for the FM and PM for acute session 3 and chronic session. The left figures display the FM mixing term results for the Acute third session and Chronic session. The mixing term term accounts for the inter- and intra-regional connectivity. The legend displays tints of red for significant positive parameter estimates and the significant negative parameter estimates are colored in tints of blue. The right figures display the PM mixing term results for the Acute third session and Chronic session. The coloring scheme is the same as the FM. These figures are symmetric within each model because the graphs are undirected.

539 Finally, across all imaging sessions the GWESP parameter estimate was reduced in magnitude (see
 540 Table 2 and 3) by the addition of the structural terms, with the largest difference seen in third acute session
 541 (see Table 3). Additionally, the GOF (see Figure 6) are fit for every statistic in all of the FM. All the GOF
 542 terms fit well except for a portion of the edge shared partners, but in the model statistics (the far right in
 543 Figure 6) are well fit to the original data.

544 As we will discuss below, the differences we are reporting between the results obtained with the
 545 conventional model (i.e., PM), estimated from functional connectivity alone, and those obtained with the
 546 full model (i.e., FM), estimated from both the functional and structural connectivity, demonstrates the risk
 547 of drawing spurious conclusions when relying on the partial model.

548 3.3 STERGM

549 The Temporal Separable ERGM (STERGM) allowed us to look at the temporal dynamics of recovery
 550 post severe brain injury with two parallel models: a formation model and a dissolution model. The formation
 551 model produces parameter estimates describing how likely it is that new connections (i.e., edges) form

	<i>ERGM Parameter Estimates</i>			
	<i>First Acute</i>		<i>Second Acute</i>	
	PM	FM	PM	FM
Edges	-6.29*** (0.28)	-6.34*** (0.56)	-7.64*** (0.36)	-7.71*** (0.59)
Nodal Covariate: Degree (Structural)		0.00 (0.00)		0.00 (0.01)
Nodal Covariate: Local Efficiency (Structural)		0.10 (0.44)		0.35 (0.35)
Nodal Covariate: Cluster Coefficient (Structural)		-0.08 (0.34)		-0.33 (0.29)
Nodal Covariate Mixing: Latent Cluster 1 to 1 (Structural)		0.03 (0.08)		1.01*** (0.15)
Nodal Covariate Mixing: Latent Cluster 2 to 2 (Structural)		0.07 (0.17)		0.82*** (0.11)
Nodal Covariate Mixing: Latent Cluster 1 to 3 (Structural)		-0.11 (0.08)		0.33** (0.12)
Nodal Covariate Mixing: Latent Cluster 2 to 3 (Structural)		-0.28* (0.12)		0.16 (0.11)
Nodal Covariate Mixing: Latent Cluster 3 to 3 (Structural)		0.24* (0.10)		0.91*** (0.12)
Nodal Covariate Mixing: Latent Cluster 1 to 4 (Structural)				0.23 (0.13)
Nodal Covariate Mixing: Latent Cluster 2 to 4 (Structural)				0.22 (0.12)
Nodal Covariate Mixing: Latent Cluster 3 to 4 (Structural)				-0.09 (0.12)
Nodal Covariate Mixing: Latent Cluster 4 to 4 (Structural)				0.86*** (0.13)
GWESP (Fixed 0.45)	2.09*** (0.13)	2.07*** (0.13)	3.11*** (0.21)	2.94*** (0.20)

Note:

* $p < 0.05$; ** $p < 0.01$; *** $p < 0.001$

Table 2. Patient recovery ERGM. Parameter estimates for the FM and PM of the Acute first and second sessions. The mixing term for resting state are excluded because they are in Figure 4. All of the structural parameter estimates are listed in the FM columns. The edges and GWESP parameter estimates are for the functional connectivity in the PMs and FMs. The LATEX code to create this table was produced by the R package called texreg (Leifeld, 2013)

	ERGM Parameter Estimates			
	Third Acute		Chronic	
	PM	FM	PM	FM
Edges	-7.97*** (0.36)	-7.27*** (0.63)	-8.05*** (0.42)	-8.07*** (0.57)
Nodal Covariate: Degree (Structural)		-0.01 (0.01)		0.01 (0.01)
Nodal Covariate: Local Efficiency (Structural)		0.02 (0.12)		-0.11 (0.16)
Nodal Covariate: Cluster Coefficient (Structural)		-0.22 (0.15)		0.33 (0.17)
Nodal Covariate Mixing: Latent Cluster 1 to 1 (Structural)		2.33*** (0.42)		0.34 (0.24)
Nodal Covariate Mixing: Latent Cluster 2 to 2 (Structural)		1.17*** (0.23)		-0.06 (0.24)
Nodal Covariate Mixing: Latent Cluster 1 to 3 (Structural)		-0.48 (0.44)		-0.34* (0.17)
Nodal Covariate Mixing: Latent Cluster 2 to 3 (Structural)		0.47* (0.23)		-0.51*** (0.17)
Nodal Covariate Mixing: Latent Cluster 3 to 3 (Structural)		1.24*** (0.24)		0.29 (0.15)
Nodal Covariate Mixing: Latent Cluster 1 to 4 (Structural)		1.25*** (0.26)		-0.52*** (0.20)
Nodal Covariate Mixing: Latent Cluster 2 to 4 (Structural)		0.35 (0.24)		-0.55*** (0.19)
Nodal Covariate Mixing: Latent Cluster 3 to 4 (Structural)		0.35 (0.23)		-0.55*** (0.16)
Nodal Covariate Mixing: Latent Cluster 4 to 4 (Structural)		1.11*** (0.23)		0.56** (0.18)
Nodal Covariate Mixing: Latent Cluster 1 to 5 (Structural)		-0.35 (0.51)		-0.20 (0.20)
Nodal Covariate Mixing: Latent Cluster 2 to 5 (Structural)		-0.01 (0.26)		-0.26 (0.20)
Nodal Covariate Mixing: Latent Cluster 3 to 5 (Structural)		0.27 (0.26)		-0.52*** (0.17)
Nodal Covariate Mixing: Latent Cluster 4 to 5 (Structural)		0.16 (0.26)		-0.39* (0.19)
Nodal Covariate Mixing: Latent Cluster 5 to 5 (Structural)		2.09*** (0.31)		0.42 (0.23)
Nodal Covariate Mixing: Latent Cluster 1 to 6 (Structural)		1.20*** (0.30)		-0.42* (0.20)
Nodal Covariate Mixing: Latent Cluster 2 to 6 (Structural)		0.60* (0.24)		-0.37* (0.18)
Nodal Covariate Mixing: Latent Cluster 3 to 6 (Structural)		-0.95* (0.40)		-0.23 (0.16)
Nodal Covariate Mixing: Latent Cluster 4 to 6 (Structural)		0.39 (0.24)		-0.22 (0.17)
Nodal Covariate Mixing: Latent Cluster 5 to 6 (Structural)		0.37 (0.29)		-0.03 (0.18)
Nodal Covariate Mixing: Latent Cluster 6 to 6 (Structural)		1.74*** (0.29)		0.30 (0.19)
Nodal Covariate Mixing: Latent Cluster 1 to 7 (Structural)		-0.54 (0.51)		
Nodal Covariate Mixing: Latent Cluster 2 to 7 (Structural)		0.42 (0.24)		
Nodal Covariate Mixing: Latent Cluster 3 to 7 (Structural)		0.28 (0.25)		
Nodal Covariate Mixing: Latent Cluster 4 to 7 (Structural)		-0.15 (0.27)		
Nodal Covariate Mixing: Latent Cluster 5 to 7 (Structural)		0.59* (0.26)		
Nodal Covariate Mixing: Latent Cluster 6 to 7 (Structural)		0.30 (0.27)		
Nodal Covariate Mixing: Latent Cluster 7 to 7 (Structural)		1.48*** (0.26)		
GWESP (Fixed 0.45)	3.23*** (0.20)	2.87*** (0.20)	3.48*** (0.24)	3.28*** (0.24)

Note:

*p<0.05; **p<0.01; ***p<0.001

Table 3. Patient Recovery ERGM. Parameter estimates for the FM and PM of the Acute third session and Chronic session. The mixing term for resting state are excluded because they are in Figure 5. All of the structural parameter estimates are listed in the FM columns. The edges and GWESP parameter estimates are for the functional connectivity in the PMs and FMs. The LATEX code to create this table was produced by the R package called texreg (Leifeld, 2013).

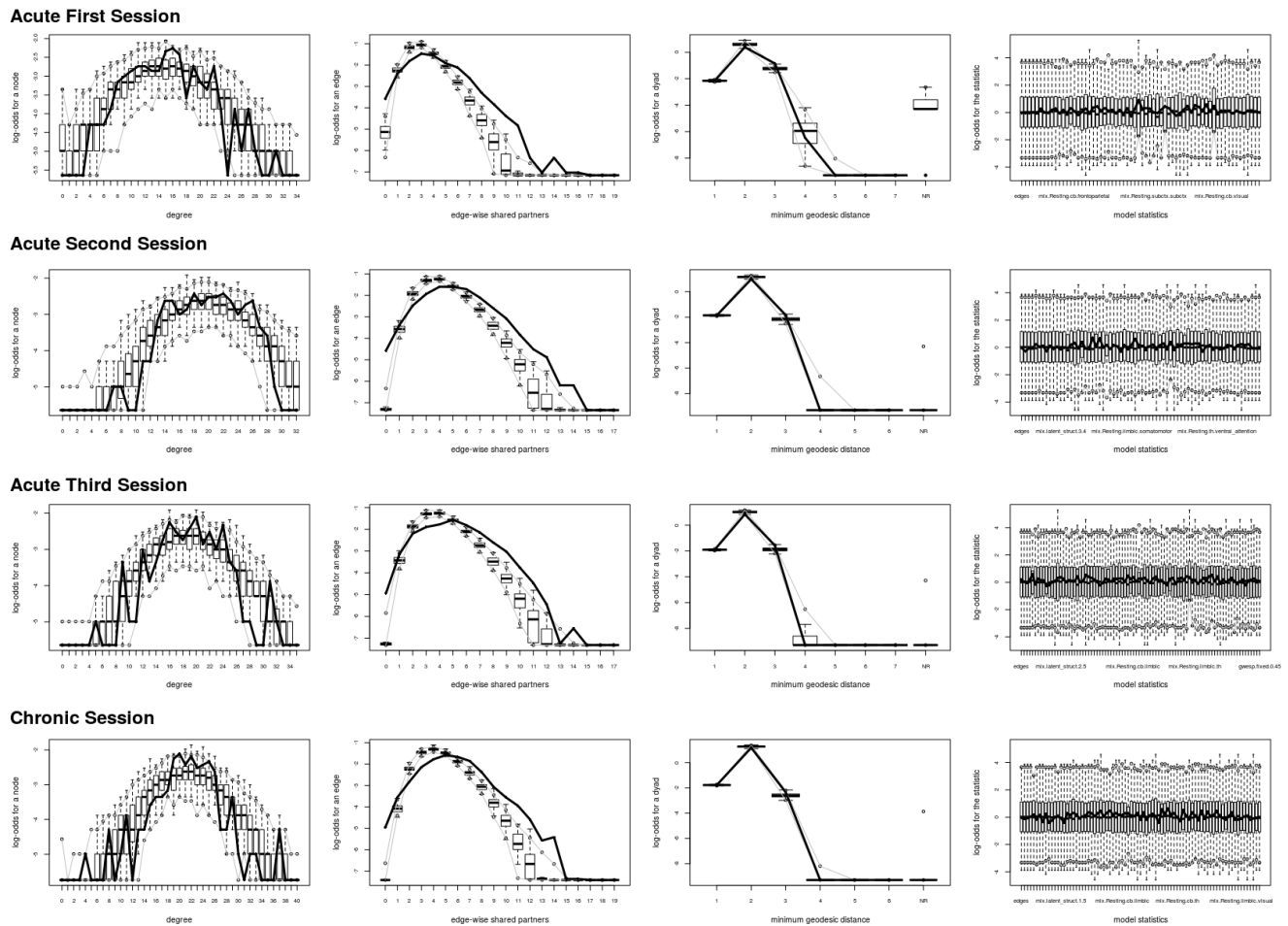


Figure 6. Patient recovery ERGM. Goodness of fit plots for the four FM (i.e., Acute Session 1, Acute Session 2, Acute Session 3 and Chronic Session). The black line marks the respective networks; the box-and-whiskers indicate the model data obtained from the 1000 simulations of each model (see section §2.6)

552 throughout the recovery from coma, while the dissolution model produces parameter estimates describing
 553 how likely it is that existing connections dissolve (or persist) throughout recovery.

554 In our index patient, the formation model showed a significant negative edges parameter estimate
 555 and a significant positive GWESP parameter estimate, the latter implying a tendency to form edges over
 556 time that close triangles (see Table 4). Additionally, none of the structural nodal covariates were found
 557 to be significant (see Table 4). There were, however, four significantly positive parameter estimates for
 558 intra-regional connectivity (i.e., default network, frontoparietal network, thalamus, and visual network; see
 559 left Figure 7), three significantly negative parameter estimates for inter-regional connectivity (i.e., between
 560 default network and visual network, somatomotor network and frontoparietal network, and ventral attention
 561 network and visual network; see left Figure 7), and two significantly positive parameter estimates for inter-
 562 regional connectivity (i.e., between default network and thalamus, and somatomotor network and ventral
 563 attention network; see left Figure 7). The dissolution model has a significantly negative edges parameter
 564 estimate and significantly positive GWESP parameter estimate (see Table 4). Also, none of the structural
 565 terms were significant for the dissolution model. Additionally, all ten parameter estimates for intra-regional

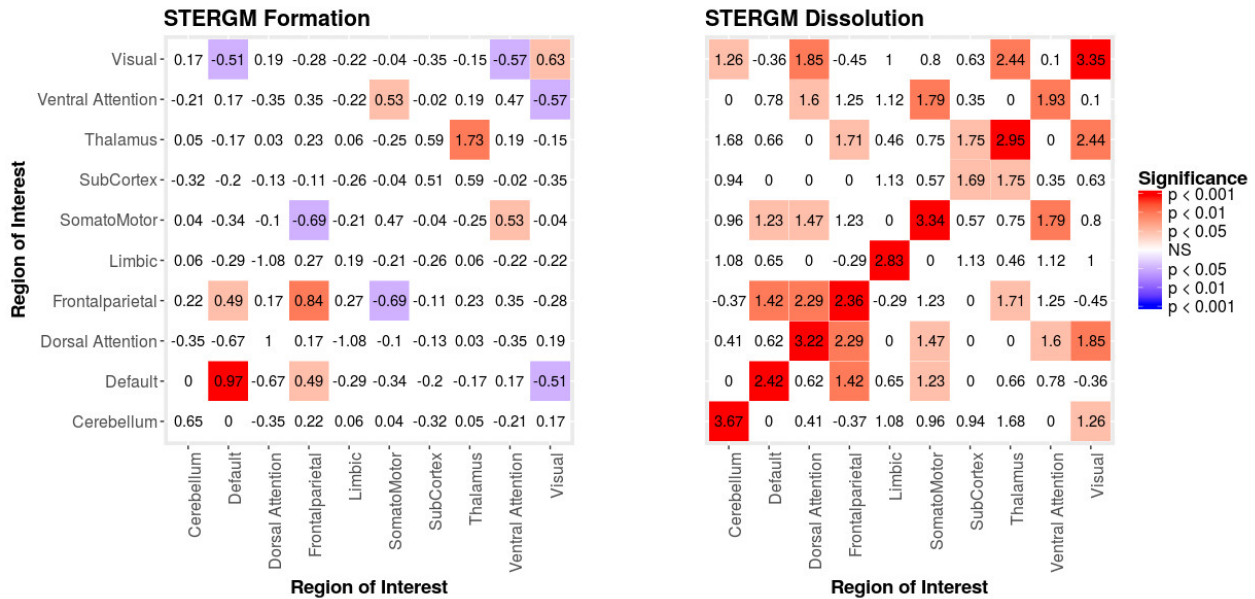


Figure 7. Patient Recovery STERGM. Results for the formation (left) and dissolution (right) models over 6 months. The mixing term term accounts for the inter- and intra-regional connectivity that form over 6 months. The legend displays tints of red for significant positive parameter estimates and the significant negative parameter estimates are colored in tints of blue. The right figure displays the dissolution model STERGM mixing term results. The coloring scheme is the same as the formation model, but the mixing term represents the connectivity that are dissolved or preserved over 6 months. These figures are symmetric within each model because the graphs are undirected.

566 connectivity (i.e., cerebellum, default network, dorsal attention network, frontoparietal network, limbic
 567 network, somatomotor network, subcortex, thalamus, ventral attention network, and visual network)
 568 significantly positive (see right Figure 7) and 11 significantly positive parameter estimates for inter-regional
 569 connectivity (i.e., between cerebellum and visual network, default network and frontoparietal network,
 570 dorsal attention network and frontoparietal network, dorsal attention network and somatomotor network,
 571 dorsal attention network and ventral attention network, dorsal attention network and visual network,
 572 frontoparietal network and thalamus, somatomotor network and ventral attention network, subcortex and
 573 thalamus, and thalamus and visual network; see right Figure 7). Finally, the GOF (see Figure 8) were fit
 574 well for every statistic in both the formation and dissolution model. Overall, the model was thus well fit
 575 for both the formation and dissolution models. All the GOF terms fit well except for a portion of the edge
 576 shared partners, but in the model statistics are well fit to the original data.

4 DISCUSSION

577 In this work, we have addressed four issues which, while general to the implementation of network theory in
 578 the field of functional neuroimaging, are particularly relevant to studies in the clinical context of disorders
 579 of consciousness. In what follows we discuss how the novel (for this field) approach we have demonstrated
 580 above in a patient recovering from coma resolves specifically each of the four problems outlined in the
 581 introduction.

	<i>STERGM Parameter Estimates</i>	
	Formation	Dissolution
Edges	−10.03*** (1.04)	−3.56* (1.79)
Nodal Covariate: Degree (Structural)	0.01 (0.01)	0.03 (0.02)
Nodal Covariate: Local Efficiency (Structural)	−0.14 (0.64)	−1.27 (1.64)
Nodal Covariate: Cluster Coefficient (Structural)	0.34 (0.49)	1.33 (1.25)
Nodal Covariate Mixing: Latent Cluster 1 to 1 (Structural)	−0.04 (0.09)	−0.01 (0.21)
Nodal Covariate Mixing: Latent Cluster 2 to 2 (Structural)	0.04 (0.17)	0.30 (0.41)
Nodal Covariate Mixing: Latent Cluster 1 to 3 (Structural)	−0.12 (0.09)	−0.11 (0.24)
Nodal Covariate Mixing: Latent Cluster 2 to 3 (Structural)	−0.04 (0.11)	0.19 (0.32)
Nodal Covariate Mixing: Latent Cluster 3 to 3 (Structural)	−0.00 (0.14)	−0.13 (0.32)
GWESP (Fixed 0.75)	3.26*** (0.33)	
GWESP (Fixed 0.25)		0.27*** (0.08)

Note:

* $p < 0.05$; ** $p < 0.01$; *** $p < 0.001$

Table 4. Patient Recovery STERGM. Parameter estimates for the formation and dissolution models. The mixing term for resting state are excluded because they are in Figure 7. All of the structural parameter estimates are listed in the FM columns. The edges and GWESP parameter estimates are for the functional connectivity in the formation and dissolution models. The LATEX code to create this table was produced by the R package called texreg (Leifeld, 2013).

582 4.1 Solution to problem #1: Use natural density, not arbitrarily fixed density (i.e., use a 583 multiple regression framework – Part I)

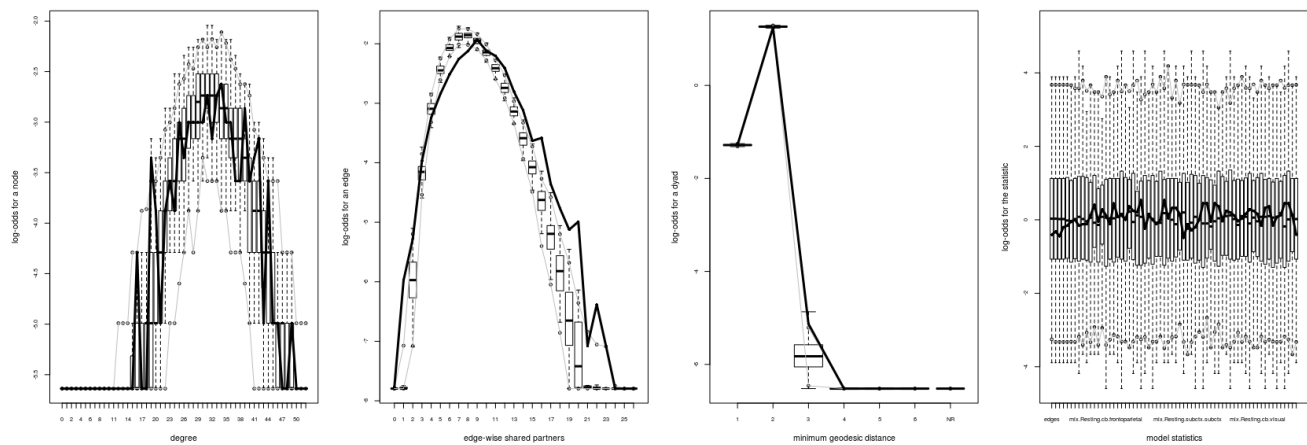
584 As our longitudinal data shows, consistent with results from other domains of neuroscience (see
585 Milham et al., 2012; Nielsen et al., 2013), brain graphs are susceptible to having different “natural” levels
586 of density at which they are the most stable and which might thus be ideal to estimate network properties.
587 In our data, over the progression of 6 months post injury, as the patient recovered consciousness and
588 cognitive function, the natural brain graph density went from 10.4% to 14.5%. These density differences
589 were revealed thanks to the use of MoNeT (Narayan et al., 2015), a tool which combines a penalized
590 maximum likelihood estimation with a resampling-based (bootstrapped) model selection procedure in
591 order to find the most stable level of sparse brain graph given a set of time-dependent measurements (e.g.,
592 fMRI data). On the one hand, as we will explain below, these differences might well reflect important
593 aspects of network dynamics in the recovery of consciousness post severe brain injury. On the other hand,
594 regardless of the ultimate interpretation of the finding in of itself, had we employed the standard approach
595 and enforced equal density across brain graphs in order to allow comparability (Rubinov and Sporns, 2010;
596 van Wijk et al., 2010), these differences would have been obscured and would have introduced a bias in

597 the direct comparison of topological properties across graphs. Ultimately, an accurate estimation of the
 598 connectivity is necessary to correctly model the connectivity. ERGM and STERGM allow for controlling
 599 the density without having to fix the density for all graphs. This allows for data driven approaches to allow
 600 the density to vary based on the stability of the connectivity estimates. This natural variance could reveal
 601 differences in graph statistics that would otherwise be masked by fixing density. Overall, this result further
 602 demonstrates that, when arbitrarily enforcing equal density across graphs, we are in fact biasing our results
 603 towards the graphs with natural density closest to the threshold employed. While we show this in the
 604 context of time, it immediately translates to cross-sectional analyses that are also typical of the field of
 605 DoC (e.g., healthy controls versus patients), with the prediction that the more different the natural density
 606 across groups, the greater the bias in the results.

607 4.2 Solution to problem #2: Control for interrelations across network metrics (i.e., use a 608 multiple regression framework – Part II)

609 As discussed above, ERGM can cope with comparing graphs with different natural densities because
 610 it factors in density as a variable in the model (in other words, it controls explicitly for different densities).

STERGM Formation



STERGM Dissolution

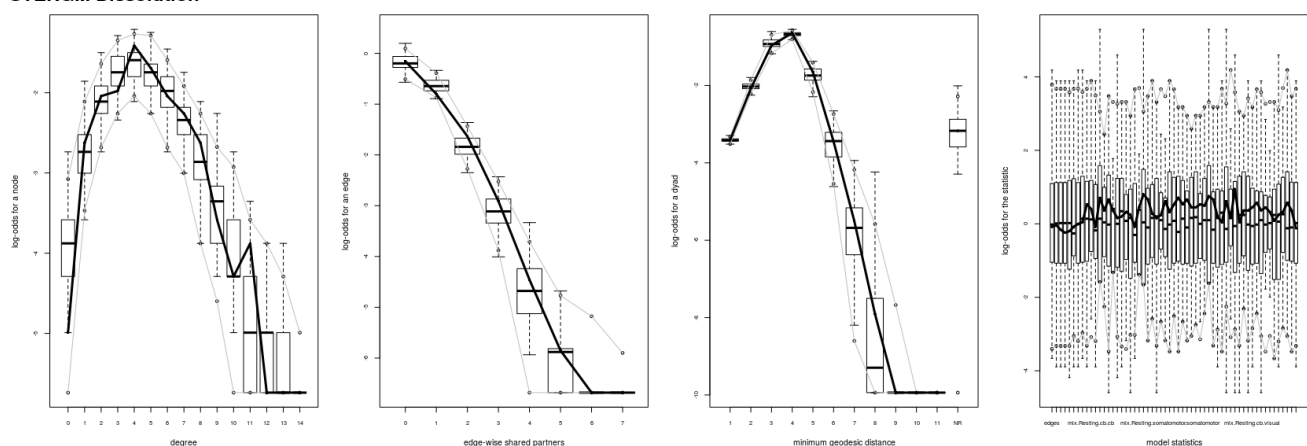


Figure 8. Patient recovery STERGM. Goodness of fit plots for the formation (top) and dissolution (bottom) models. The black line marks the formation and dissolution networks observed over time in the patient's graphs between the first Acute session and the Chronic session; the box-and-wiskers indicate the model data obtained from the 1000 simulations of each model (see section §2.6)

611 Similarly, ERGM can also control for interrelations across the many metrics that are typically estimated
612 by explicitly including them all in a single model. As mentioned in the introduction, this approach is
613 akin to performing a multiple regression model in which each network feature is evaluated for its unique
614 contribution to the graph, as opposed to the current graph theoretic approach dominating in neuroimaging,
615 which is akin to running several single-variable regressions, one per topological feature investigated. The
616 Florentine business networks were used to demonstrate the effect of leaving out significant contributing
617 factors to the model, something that renders our ERGM vulnerable to correlations between graph properties
618 similar to the current conventional approach (Rubinov and Sporns, 2010). As shown in Table 1, using
619 partial models can lead to incorrectly estimating the magnitude or the significance of network measures.
620 For example, in network A (Figure 1, left), the failure to include the mixing terms leads to a significant
621 GWESP term, however, it appears to be overestimated as compared to the FM (where it is not significant).
622 In other words, on the basis of the partial model results, one would be justified in concluding that triadic
623 closure (i.e., the tendency for edges to appear where they complete triangles) is a key stochastic process
624 underlying the network. Yet, the FM shows that this result is spurious and is in fact due to the mixing
625 term – that is, to the dynamics of within-group connectivity, and not triadic closure. As shown in Table 1,
626 changing group membership of one node alone, preserving all other aspects of the network, affected both
627 qualitatively and quantitatively the network measures (compare the FM columns for PM_A and PM_B in
628 Table 1). Similarly to Network A, Network B's partial models returned different parameter estimates than
629 the FM. As we will discuss below, a similar effect is at play in the neuroimaging data where, failure to
630 include structural information, could have led to incorrectly attributing to functional connectivity between
631 the fronto-parietal and the default mode networks a network characteristic that is in fact due to structural
632 connectivity (i.e., problem #3, cf., Figures 4 and 5).

633 4.3 Solution to problem #3: Adjust for the effects of structural connectivity on 634 functional connectivity (i.e., use a multiple regression framework – Part III)

635 As shown in the results, ERGM is capable of addressing the currently unresolved issue of integrating
636 functional and structural connectivity in a unique framework (Hunter, 2007; Hunter et al., 2008; Handcock
637 et al., 2017). Analogously to the two previous points, the solution employed by ERGM is to include
638 structural connectivity terms in the model, thus explicitly adjusting for the relationship between the
639 structural and functional connectivity. In our data, inclusion of structural terms in the model affected all
640 other parameter estimates, empirically demonstrating that, in the context of recovery of consciousness after
641 severe brain injury, failing to include structural connectivity is tantamount to mis-specifying the model
642 (similarly to not including network density [i.e., problem #1] or not modeling all estimated metrics in a
643 single model [i.e., problem #2]). While we recognize that this is likely to be an issue in any field where
644 structural connectivity might differ across groups and/or individuals, there is also little doubt that this
645 is particularly problematic in the context of disorders of consciousness where the underlying structural
646 architecture is likely to be substantially different from healthy volunteers (e.g. Lutkenhoff et al., 2015;
647 Fernández-Espejo et al., 2011), across different clinical groups (e.g. Zheng et al., 2017), and over time (e.g.
648 Lutkenhoff et al., 2013; Thengone et al., 2016, as well as in the data presented here).

649 Specifically, our results show that when structural data are included (i.e., in the FMs), the probability
650 of inter- and intra-regional connectivity changes – as compared to the PMs – including: parameter estimates
651 with a higher magnitude in the PM (e.g., connections between default network and ventral attention
652 network, limbic network to thalamus, and within limbic network in the Acute First session), parameters
653 with a lower magnitude in PM (e.g., connections between visual network and cerebellum, visual network
654 and subcortex or visual network and thalamus in the Acute Second session), and parameters which went

655 from non-significant in the PM to significant in the FM (e.g., connections between dorsal attention network
656 and subcortex in the Acute Second session or connections between visual network and ventral attention in
657 the Chronic session) and viceversa (e.g., connections between default network and frontoparietal network
658 in the Chronic session or connections between thalamus and subcortex in the Acute First session). These
659 results have immediate theoretical implications for the field of disorders of consciousness in as much as
660 the partial ERGM model in our patient shows increased likelihood of connectivity between the default
661 mode and the fronto-parietal networks throughout recovery from coma (see Figure 4 and 5). This could be
662 (mistakenly) construed as bearing on the issue of the relationship between the “external awareness” and
663 “internal awareness” networks in disorders of consciousness (Boly et al., 2008a,b). For, the relationship
664 between these two networks was no longer observed once structural data was included in the FM exposing
665 the initial finding as spurious and likely reflecting improper attribution of variance due to leaving out the
666 structural terms from the model.

667 Finally, we note that ERGM has an important advantage over other techniques in the context of
668 integrating functional and structural connectivity. Indeed, previous approaches only made use of the
669 structural connectivity in order to predict the functional network (Bettinardi et al., 2017; Messé et al., 2015)
670 or in order to jointly estimate the functional and structural connectivity (Kessler et al., 2014; Mišić et al.,
671 2016; Amico and Goñi, 2017). ERGM, however, allows estimating the influence of structural connectivity
672 on the properties of the functional networks, something which, even at the level of one patient alone, has a
673 large enough effect to change the significance and/or magnitude of the network’s parameter estimates.

674 **4.4 Solution to problem #4: Assess dynamics of change across time-points, not static** 675 **differences across time-points**

676 Finally, an additional advantage of this new approach, is the ability to directly analyze network
677 dynamics over time – an issue that is very important in the context of loss and recovery of consciousness
678 after severe brain injury (Laureys et al., 2000b; Crone et al., 2017a). In our example data, the two STERGM
679 models uncovered a strong positive parameter estimates for intra-regional connectivity in all networks, for
680 the dissolution model, indicating that in the process of recovery there are strong tendencies to preserve
681 existing edges across time. Additionally, there are four positive parameter estimates for the formation of
682 new edges, implying that as our patient recovered he was more likely to establish new connectivity within
683 and between networks. Taken together, the tendency of our patient to maintain existing connections and
684 develop novel ones might well explain why we observed a tendency over time for the “natural” density
685 of networks to increase throughout recovery. It should also be pointed out that while we did not find any
686 negative parameter estimate in the dissolution model, a significant negative estimate could be interpreted as
687 evidence for neural reorganization, another important advantage of ERGM in the context of disorders of
688 consciousness (e.g., Voss et al., 2006).

5 CONCLUSIONS AND FUTURE WORK

689 Network analyses are an attempt to synthesize complex processes into a small number of metrics. In
690 this paper we have introduced a novel (in the context of DOC, for other contexts within neuroimaging,
691 cf.: Simpson et al., 2011, 2012, 2013) approach to estimating network properties, Exponential Random
692 Graph Models, which overcome four important challenges faced by current graph theoretic approaches to
693 brain data and which are particularly consequential in the context of disorders of consciousness. The main
694 advantage of ERGM over current approaches is the fact that it adopts a multiple regression framework
695 *in lieu* of multiple parallel simple regressions (i.e., one per each metric). Under this multiple regression

696 framework, brain networks can be compared across densities – since the density of each will be controlled
697 for within the model. This side-steps the issue of having to impose the same arbitrary sparsity across
698 networks which are likely to have very different stable levels of density, as is the case, for example,
699 between severely brain injured patients and controls or in longitudinal recovery. Similarly, by including
700 in a unified model structural and functional data, it is possible to acknowledge and control for the fact
701 that patients surviving severe brain injury are likely to have very heterogeneous brain pathology and thus
702 profound differences in structural substrate – a fact that is currently ignored in the extant literature. Even in
703 one patient alone, direct comparison of the conventional partial model with the full model demonstrated
704 how failing to consider structural information can lead to spurious results and erroneous conclusions.
705 Furthermore, ERGM can be extended to assess dynamics of change thus allowing to discover the network
706 evolution that govern loss and recovery of consciousness over time, as opposed to comparing static graphs
707 at different time-points.

708 Finally, we end this paper by pointing out that the reader can implement (ST)ERGM as performed
709 here using the freely distributed `ergm` package (Handcock et al., 2017) in R and the Markov Network
710 Toolbox (MoNeT; Narayan et al., 2015) in MATLAB.

FUNDING

711 This work was supported by the Tiny Blue Dot foundation (to MMM) and the Brain Injury Research Center
712 at UCLA.

REFERENCES

- 713 Abdi, H. (2010). Partial least squares regression and projection on latent structure regression (PLS
714 regression). *Wiley Interdisciplinary Reviews: Computational Statistics* 2, 97–106. doi:10.1002/wics.51
- 715 Abou-Elseoud, A., Starck, T., Remes, J., Nikkinen, J., Tervonen, O., and Kiviniemi, V. (2010). The effect
716 of model order selection in group PICA. *Human brain mapping* 31, 1207–1216
- 717 Amico, E. and Goñi, J. (2017). Mapping hybrid functional-structural connectivity traits in the human
718 connectome. *arXiv preprint arXiv:1710.02199*
- 719 Amico, E., Marinazzo, D., Di Perri, C., Heine, L., Annen, J., Martial, C., et al. (2017). Mapping the
720 functional connectome traits of levels of consciousness. *NeuroImage* 148, 201–211
- 721 Avants, B. B., Epstein, C. L., Grossman, M., and Gee, J. C. (2008). Symmetric diffeomorphic image
722 registration with cross-correlation: evaluating automated labeling of elderly and neurodegenerative brain.
723 *Medical image analysis* 12, 26–41
- 724 Avants, B. B., Tustison, N. J., Song, G., Cook, P. A., Klein, A., and Gee, J. C. (2011). A reproducible
725 evaluation of ANTs similarity metric performance in brain image registration. *NeuroImage* 54, 2033–
726 2044
- 727 Averbeck, B. B. and Seo, M. (2008). The statistical neuroanatomy of frontal networks in the macaque.
728 *PLoS computational biology* 4, e1000050
- 729 Baars, B. J. (2002). The conscious access hypothesis: origins and recent evidence. *Trends in cognitive
730 sciences* 6, 47–52
- 731 Baars, B. J., Ramsøy, T. Z., and Laureys, S. (2003). Brain, conscious experience and the observing self.
732 *Trends in neurosciences* 26, 671–675
- 733 Barttfeld, P., Uhrig, L., Sitt, J. D., Sigman, M., Jarraya, B., and Dehaene, S. (2015). Signature of
734 consciousness in the dynamics of resting-state brain activity. *Proceedings of the National Academy of
735 Sciences* 112, 887–892

- 736 Behrens, T. E., Berg, H. J., Jbabdi, S., Rushworth, M. F., and Woolrich, M. W. (2007). Probabilistic
737 diffusion tractography with multiple fibre orientations: What can we gain? *Neuroimage* 34, 144–155
- 738 Behrens, T. E., Woolrich, M. W., Jenkinson, M., Johansen-Berg, H., Nunes, R. G., Clare, S., et al. (2003).
739 Characterization and propagation of uncertainty in diffusion-weighted MR imaging. *Magnetic resonance*
740 *in medicine* 50, 1077–1088
- 741 Bettinardi, R. G., Deco, G., Karlaftis, V. M., Van Hartevelt, T. J., Fernandes, H. M., Kourtzi, Z., et al.
742 (2017). How structure sculpts function: Unveiling the contribution of anatomical connectivity to the
743 brain's spontaneous correlation structure. *Chaos: An Interdisciplinary Journal of Nonlinear Science* 27,
744 047409
- 745 Bhushan, C., Haldar, J. P., Joshi, A. A., and Leahy, R. M. (2012). Correcting susceptibility-induced
746 distortion in diffusion-weighted MRI using constrained nonrigid registration. *Signal and Information*
747 *Processing Association Annual Summit and Conference (APSIPA), ... Asia-Pacific. Asia-Pacific Signal*
748 *and Information Processing Association Annual Summit and Conference 2012*
- 749 Boly, M., Garrido, M. I., Gosseries, O., Bruno, M.-A., Boveroux, P., Schnakers, C., et al. (2011). Preserved
750 feedforward but impaired top-down processes in the vegetative state. *Science* 332, 858–862
- 751 Boly, M., Massimini, M., Garrido, M. I., Gosseries, O., Noirhomme, Q., Laureys, S., et al. (2012a). Brain
752 connectivity in disorders of consciousness. *Brain connectivity* 2, 1–10
- 753 Boly, M., Moran, R., Murphy, M., Boveroux, P., Bruno, M.-A., Noirhomme, Q., et al. (2012b). Connectivity
754 changes underlying spectral EEG changes during propofol-induced loss of consciousness. *Journal of*
755 *Neuroscience* 32, 7082–7090
- 756 Boly, M., Phillips, C., Balteau, E., Schnakers, C., Degueldre, C., Moonen, G., et al. (2008a). Consciousness
757 and cerebral baseline activity fluctuations. *Human brain mapping* 29, 868–874. doi:10.1002/hbm.20602
- 758 Boly, M., Phillips, C., Tshibanda, L., Vanhauzenhuyse, A., Schabus, M., Dang-Vu, G., T. T. Moonon, et al.
759 (2008b). Intrinsic brain activity in altered states of consciousness. *Annals of the New York Academy of*
760 *Sciences* 1129, 119–129. doi:10.1196/annals.1417.015
- 761 Boly, M., Tshibanda, L., Vanhauzenhuyse, A., Noirhomme, Q., Schnakers, C., Ledoux, D., et al. (2009).
762 Functional connectivity in the default network during resting state is preserved in a vegetative but not in
763 a brain dead patient. *Human brain mapping* 30, 2393–2400
- 764 Boveroux, P., Vanhauzenhuyse, A., Bruno, M.-A., Noirhomme, Q., Lauwick, S., Luxen, A., et al.
765 (2010). Breakdown of within-and between-network resting state functional magnetic resonance imaging
766 connectivity during propofol-induced loss of consciousness. *Anesthesiology: The Journal of the American*
767 *Society of Anesthesiologists* 113, 1038–1053
- 768 Braitenberg, V. and Schüz, A. (1998). Global activity, cell assemblies and synfire chains. In *Cortex:*
769 *Statistics and Geometry of Neuronal Connectivity* (Springer). 193–204
- 770 Braun, U., Plichta, M. M., Esslinger, C., Sauer, C., Haddad, L., Grimm, O., et al. (2012). Test–retest
771 reliability of resting-state connectivity network characteristics using fMRI and graph theoretical measures.
772 *Neuroimage* 59, 1404–1412
- 773 Bruno, M.-A., Fernández-Espejo, D., Lehembre, R., Tshibanda, L., Vanhauzenhuyse, A., Gosseries, O.,
774 et al. (2011). Multimodal neuroimaging in patients with disorders of consciousness showing “functional
775 hemispherectomy”. In *Progress in brain research* (Elsevier), vol. 193. 323–333
- 776 Buckner, R. L. (2010). Human functional connectivity: new tools, unresolved questions. *Proceedings of*
777 *the National Academy of Sciences* 107, 10769–10770. doi:10.1073/pnas.1005987107
- 778 Bullmore, E. and Sporns, O. (2012). The economy of brain network organization. *Nature Reviews*
779 *Neuroscience* 13, 336–349

- 780 Calhoun, V. D., Adali, T., Giuliani, N. R., Pekar, J. J., Kiehl, K. A., and Pearlson, G. D. (2006). Method for
781 multimodal analysis of independent source differences in schizophrenia: combining gray matter structural
782 and auditory oddball functional data. *Human brain mapping* 27, 47–62. doi:10.1002/hbm.20166
- 783 Calhoun, V. D., Liu, J., and Adali, T. (2009). A review of group ICA for fMRI data and ICA for joint
784 inference of imaging, genetic, and ERP data). *Neuroimage* 45, S163–S172. doi:10.1016/j.neuroimage.
785 2008.10.057
- 786 Cao, H., Plichta, M. M., Schäfer, A., Haddad, L., Grimm, O., Schneider, M., et al. (2014). Test–retest
787 reliability of fMRI-based graph theoretical properties during working memory, emotion processing, and
788 resting state. *Neuroimage* 84, 888–900
- 789 Chennu, S., Finoia, P., Kamau, E., Allanson, J., Williams, G. B., Monti, M. M., et al. (2014). Spectral
790 signatures of reorganised brain networks in disorders of consciousness. *PLoS computational biology* 10,
791 e1003887
- 792 Cohen, A. L., Fair, D. A., Dosenbach, N. U., Miezin, F. M., Dierker, D., Van Essen, D. C., et al.
793 (2008). Defining functional areas in individual human brains using resting functional connectivity MRI.
794 *Neuroimage* 41, 45–57
- 795 Coleman, M., Bekinschtein, T., Monti, M., Owen, A., and Pickard, J. (2009). A multimodal approach to
796 the assessment of patients with disorders of consciousness. *Progress in brain research* 177, 231–248
- 797 Craddock, R. C., James, G. A., Holtzheimer, P. E., Hu, X. P., and Mayberg, H. S. (2012). A whole brain
798 fMRI atlas generated via spatially constrained spectral clustering. *Human brain mapping* 33, 1914–1928
- 799 Crick, F. and Koch, C. (2003). A framework for consciousness. *Nature neuroscience* 6, 119–126
- 800 Crone, J. S., Bio, B. J., Vespa, P. M., Lutkenhoff, E. S., and Monti, M. M. (2017a). Restoration of
801 thalamo-cortical connectivity after brain injury: recovery of consciousness, complex behavior, or passage
802 of time? *Journal of neuroscience research* , [Advance online ePub].
- 803 Crone, J. S., Lutkenhoff, E. S., Bio, B. J., Laureys, S., and Monti, M. M. (2017b). Testing proposed
804 neuronal models of effective connectivity within the cortico-basal ganglia-thalamo-cortical loop during
805 loss of consciousness. *Cerebral Cortex* 27, 2727–2738
- 806 Crone, J. S., Soddu, A., Höller, Y., Vanhaudenhuyse, A., Schurz, M., Bergmann, J., et al. (2014).
807 Altered network properties of the fronto-parietal network and the thalamus in impaired consciousness.
808 *NeuroImage: Clinical* 4, 240–248
- 809 Dehaene, S. and Changeux, J.-P. (2005). Ongoing spontaneous activity controls access to consciousness: a
810 neuronal model for inattentive blindness. *PLoS biology* 3, e141
- 811 Díaz-Parra, A., Osborn, Z., Canals, S., Moratal, D., and Sporns, O. (2017). Structural and functional,
812 empirical and modeled connectivity in the cerebral cortex of the rat. *NeuroImage* 159, 170–184
- 813 Engel, A. K. and Singer, W. (2001). Temporal binding and the neural correlates of sensory awareness.
814 *Trends in cognitive sciences* 5, 16–25
- 815 Erdős, P. and Rényi, A. (1959). On random graphs I. *Publicationes Mathematicae (Debrecen)* 6, 290–297
- 816 Fernández-Espejo, D., Bekinschtein, T., Monti, M. M., Pickard, J. D., Junque, C., Coleman, M. R., et al.
817 (2011). Diffusion weighted imaging distinguishes the vegetative state from the minimally conscious
818 state. *Neuroimage* 54, 103–112
- 819 Fernández-Espejo, D., Soddu, A., Cruse, D., Palacios, E. M., Junque, C., Vanhaudenhuyse, A., et al. (2012).
820 A role for the default mode network in the bases of disorders of consciousness. *Annals of neurology* 72,
821 335–343
- 822 Finger, H., Bönstrup, M., Cheng, B., Messé, A., Hilgetag, C., Thomalla, G., et al. (2016). Modeling of
823 large-scale functional brain networks based on structural connectivity from DTI: comparison with EEG

- 824 derived phase coupling networks and evaluation of alternative methods along the modeling path. *PLoS*
825 *computational biology* 12, e1005025
- 826 Fornito, A., Zalesky, A., and Breakspear, M. (2013). Graph analysis of the human connectome: promise,
827 progress, and pitfalls. *Neuroimage* 80, 426–444. doi:10.1016/j.neuroimage.2013.04.087
- 828 Fornito, A., Zalesky, A., and Bullmore, E. (2016). *Fundamentals of brain network analysis* (Academic
829 Press)
- 830 Fox, M. D., Corbetta, M., Snyder, A. Z., Vincent, J. L., and Raichle, M. E. (2006). Spontaneous neuronal
831 activity distinguishes human dorsal and ventral attention systems. *Proceedings of the National Academy*
832 *of Sciences* 103, 10046–10051. doi:10.1073/pnas.0604187103
- 833 Fransson, P., Åden, U., Blennow, M., and Lagercrantz, H. (2010). The functional architecture of the infant
834 brain as revealed by resting-state fmri. *Cerebral cortex* 21, 145–154
- 835 Freeman, L. C. (1978). Centrality in social networks conceptual clarification. *Social networks* 1, 215–239
- 836 Goodreau, S. M., Kitts, J. A., and Morris, M. (2009). Birds of a feather, or friend of a friend? using
837 exponential random graph models to investigate adolescent social networks. *Demography* 46, 103–125
- 838 Guimera, R., Mossa, S., Turtschi, A., and Amaral, L. N. (2005). The worldwide air transportation network:
839 Anomalous centrality, community structure, and cities' global roles. *Proceedings of the National*
840 *Academy of Sciences* 102, 7794–7799
- 841 Haldar, J. P. and Leahy, R. M. (2013). Linear transforms for fourier data on the sphere: Application to high
842 angular resolution diffusion MRI of the brain. *NeuroImage* 71, 233–247
- 843 Hallquist, M. N. and Hillary, F. G. (2018). Graph theory approaches to functional network organization in
844 brain disorders: A critique for a brave new small-world. *bioRxiv* , 243741
- 845 Handcock, M. S., Hunter, D. R., Butts, C. T., Goodreau, S. M., Krivitsky, P. N., and Morris, M. (2017).
846 *ergm: Fit, Simulate and Diagnose Exponential-Family Models for Networks*. The Statnet Project
847 (<http://www.statnet.org>). R package version 3.8.0
- 848 Handcock, M. S., Raftery, A. E., and Tantrum, J. M. (2007). Model-based clustering for social networks.
849 *Journal of the Royal Statistical Society: Series A (Statistics in Society)* 170, 301–354
- 850 Hannawi, Y., Lindquist, M. A., Caffo, B. S., Sair, H. I., and Stevens, R. D. (2015). Resting brain activity in
851 disorders of consciousness a systematic review and meta-analysis. *Neurology* 84, 1272–1280
- 852 Hellwig, B. (2000). A quantitative analysis of the local connectivity between pyramidal neurons in layers
853 2/3 of the rat visual cortex. *Biological cybernetics* 82, 111–121
- 854 Hernández, M., Guerrero, G. D., Cecilia, J. M., García, J. M., Inuggi, A., Jbabdi, S., et al. (2013).
855 Accelerating fibre orientation estimation from diffusion weighted magnetic resonance imaging using
856 gpus. *PloS one* 8, e61892
- 857 Holland, P. W. and Leinhardt, S. (1981). An exponential family of probability distributions for directed
858 graphs. *Journal of the american statistical association* 76, 33–50
- 859 Hunter, D. R. (2007). Curved exponential family models for social networks. *Social networks* 29, 216–230
- 860 Hunter, D. R., Handcock, M. S., Butts, C. T., Goodreau, S. M., and Morris, M. (2008). ergm: A package to
861 fit, simulate and diagnose exponential-family models for networks. *Journal of statistical software* 24,
862 nihpa54860
- 863 Hyvärinen, A. and Oja, E. (2000). Independent component analysis: algorithms and applications. *Neural*
864 *networks* 13, 411–430. doi:10.1016/S0893-6080(00)00026-5
- 865 Ioannides, A. A. (2007). Dynamic functional connectivity. *Current opinion in neurobiology* 17, 161–170.
866 doi:10.1016/j.conb.2007.03.008
- 867 Kent, D. V. (1978). *The rise of the Medici: Faction in Florence, 1426-1434* (Oxford University Press,
868 USA)

- 869 Kessler, D., Angstadt, M., Welsh, R. C., and Sripada, C. (2014). Modality-spanning deficits in attention-
870 deficit/hyperactivity disorder in functional networks, gray matter, and white matter. *Journal of*
871 *Neuroscience* 34, 16555–16566. doi:10.1523/JNEUROSCI.3156-14.2014
- 872 Krishnan, A., Williams, L. J., McIntosh, A. R., and Abdi, H. (2011). Partial least squares (PLS) methods for
873 neuroimaging: a tutorial and review. *Neuroimage* 56, 455–475. doi:10.1016/j.neuroimage.2010.07.034
- 874 Krivitsky, P. N. and Handcock, M. S. (2008). Fitting position latent cluster models for social networks with
875 latentnet. *Journal of Statistical Software* 24
- 876 Krivitsky, P. N. and Handcock, M. S. (2014). A separable model for dynamic networks. *Journal of the*
877 *Royal Statistical Society* 76, 29–46. doi:10.1111/rssb.12014
- 878 Ku, S.-W., Lee, U., Noh, G.-J., Jun, I.-G., and Mashour, G. A. (2011). Preferential inhibition of frontal-to-
879 parietal feedback connectivity is a neurophysiologic correlate of general anesthesia in surgical patients.
880 *PLoS one* 6, e25155. doi:10.1371/journal.pone.0025155
- 881 Lashkari, D., Vul, E., Kanwisher, N., and Golland, P. (2010). Discovering structure in the space of fMRI
882 selectivity profiles. *Neuroimage* 50, 1085–1098. doi:10.1016/j.neuroimage.2009.12.106
- 883 Laureys, S., Faymonville, M. E., Degueldre, C., Fiore, G. D., Damas, P., Lambermont, B., et al. (2000a).
884 Auditory processing in the vegetative state. *Brain: a journal of neurology* 123 (Pt 8), 1589–1601
- 885 Laureys, S., Faymonville, M. E., Luxen, A., Lamy, M., Franck, G., and Maquet, P. (2000b). Restoration of
886 thalamocortical connectivity after recovery from persistent vegetative state. *Lancet (London, England)*
887 355, 1790–1791
- 888 Lee, U., Kim, S., Noh, G.-J., Choi, B.-M., Hwang, E., and Mashour, G. A. (2009). The directionality and
889 functional organization of frontoparietal connectivity during consciousness and anesthesia in humans.
890 *Consciousness and cognition* 18, 1069–1078. doi:10.1016/j.concog.2009.04.004
- 891 Leifeld, P. (2013). texreg: Conversion of statistical model output in r to latex and html tables. *Journal of*
892 *Statistical Software* 55. doi:10.18637/jss.v055.i08
- 893 Lucek, P. R. and Ott, J. (1997). Neural network analysis of complex traits. *Genetic epidemiology* 14,
894 1101–1106. doi:10.1002/(SICI)1098-2272(1997)14:6<1101::AID-GEPI90>3.0.CO;2-K
- 895 Luke, D. A. and Harris, J. K. (2007). Network analysis in public health: history, methods, and applications.
896 *Annual review of public health* 28, 69–93. doi:10.1146/annurev.publhealth.28.021406.144132
- 897 Lutkenhoff, E. S., Chiang, J., Tshibanda, L., Kamau, E., Kirsch, M., Pickard, J. D., et al. (2015). Thalamic
898 and extrathalamic mechanisms of consciousness after severe brain injury. *Annals of neurology* 78, 68–76.
899 doi:10.1002/ana.24423
- 900 Lutkenhoff, E. S., McArthur, D. L., Hua, X., Thompson, P. M., Vespa, P. M., and Monti, M. M. (2013).
901 Thalamic atrophy in antero-medial and dorsal nuclei correlates with six-month outcome after severe
902 brain injury. *NeuroImage: Clinical* 3, 396–404
- 903 Lutkenhoff, E. S., Rosenberg, M., Chiang, J., Zhang, K., Pickard, J. D., Owen, A. M., et al. (2014).
904 Optimized brain extraction for pathological brains (optiBET). *PLoS one* 9, e115551. doi:10.1371/journal.
905 pone.0115551
- 906 Martuzzi, R., Ramani, R., Qiu, M., Rajeevan, N., and Constable, R. T. (2010). Functional connectivity and
907 alterations in baseline brain state in humans. *Neuroimage* 49, 823–834
- 908 McIntosh, A. R. and Lobaugh, N. J. (2004). Partial least squares analysis of neuroimaging data: applications
909 and advances. *Neuroimage* 23, S250–S263. doi:10.1016/j.neuroimage.2004.07.020
- 910 McIntosh, A. R. and Mišić, B. (2013). Multivariate statistical analyses for neuroimaging data. *Annual*
911 *review of psychology* 64, 499–525. doi:10.1146/annurev-psych-113011-143804
- 912 McQuillan, J. M. (1977). Graph theory applied to optimal connectivity in computer networks. *SIGCOMM*
913 *Computer Communications Review* 7, 13–41. doi:10.1145/1024857.1024860

- 914 Messé, A., Rudrauf, D., Giron, A., and Marrelec, G. (2015). Predicting functional connectivity from
915 structural connectivity via computational models using mri: an extensive comparison study. *NeuroImage*
916 111, 65–75. doi:10.1016/j.neuroimage.2015.02.001
- 917 Micheloyannis, S., Vourkas, M., Tsirka, V., Karakonstantaki, E., Kanatsouli, K., and Stam, C. J. (2009).
918 The influence of ageing on complex brain networks: a graph theoretical analysis. *Human brain mapping*
919 30, 200–208. doi:10.1002/hbm.20492
- 920 Mišić, B., Betzel, R. F., De Reus, M. A., Van Den Heuvel, M. P., Berman, M. G., McIntosh, A. R.,
921 et al. (2016). Network-level structure-function relationships in human neocortex. *Cerebral Cortex* 26,
922 3285–3296. doi:10.1093/cercor/bhw089
- 923 Milham, M. P., Fair, D., Mennes, M., Mostofsky, S. H., et al. (2012). The ADHD-200 consortium: a model
924 to advance the translational potential of neuroimaging in clinical neuroscience. *Frontiers in systems*
925 *neuroscience* 6, 62
- 926 Monti, M. M. (2012). Cognition in the vegetative state. *Annual review of clinical psychology* 8, 431–454
- 927 Monti, M. M., Laureys, S., and Owen, A. M. (2010). The vegetative state. *BMJ (Clinical Research ed.)*
928 341, c3765
- 929 Monti, M. M., Lutkenhoff, E. S., Rubinov, M., Boveroux, P., Vanhaudenhuyse, A., Gosseries, O.,
930 et al. (2013). Dynamic change of global and local information processing in propofol-induced loss and
931 recovery of consciousness. *PLoS computational biology* 9, e1003271. doi:10.1371/journal.pcbi.1003271
- 932 Narayan, M., Allen, G. I., and Tomson, S. (2015). Two sample inference for populations of graphical
933 models with applications to functional connectivity. *arXiv preprint arXiv:1502.03853*
- 934 Newcombe, V. F. J., Williams, G. B., Scoffings, D., Cross, J., Carpenter, T. A., Pickard, J. D., et al.
935 (2010). Aetiological differences in neuroanatomy of the vegetative state: insights from diffusion tensor
936 imaging and functional implications. *Journal of neurology, neurosurgery, and psychiatry* 81, 552–561.
937 doi:10.1136/jnnp.2009.196246
- 938 Nielsen, J. A., Zielinski, B. A., Fletcher, P. T., Alexander, A. L., Lange, N., Bigler, E. D., et al. (2013).
939 Multisite functional connectivity MRI classification of autism: Abide results. *Frontiers in human*
940 *neuroscience* 7, 599. doi:10.3389/fnhum.2013.00599
- 941 Oguz, I., Farzinfar, M., Matsui, J., Budin, F., Liu, Z., Gerig, G., et al. (2014). DTIPrep: quality control of
942 diffusion-weighted images. *Frontiers in neuroinformatics* 8. doi:10.3389/fninf.2014.00004
- 943 Pandit, A. S., Expert, P., Lambiotte, R., Bonnelle, V., Leech, R., Turkheimer, F. E., et al. (2013).
944 Traumatic brain injury impairs small-world topology. *Neurology* 80, 1826–1833. doi:10.1212/WNL.
945 0b013e3182929f38
- 946 Power, J. D., Barnes, K. A., Snyder, A. Z., Schlaggar, B. L., and Petersen, S. E. (2012). Spurious but
947 systematic correlations in functional connectivity MRI networks arise from subject motion. *NeuroImage*
948 59, 2142–2154. doi:10.1016/j.neuroimage.2011.10.018
- 949 Raichle, M. E., MacLeod, A. M., Snyder, A. Z., Powers, W. J., Gusnard, D. A., and Shulman, G. L. (2001).
950 A default mode of brain function. *Proceedings of the National Academy of Sciences of the United States*
951 *of America* 98, 676–682. doi:10.1073/pnas.98.2.676
- 952 Ray, K. L., McKay, D. R., Fox, P. M., Riedel, M. C., Uecker, A. M., Beckmann, C. F., et al. (2013). Ica
953 model order selection of task co-activation networks. *Frontiers in neuroscience* 7, 237. doi:10.3389/
954 fnins.2013.00237
- 955 Robins, G., Pattison, P., Kalish, Y., and Lusher, D. (2007). An introduction to exponential random graph
956 (p^*) models for social networks. *Social Networks* 29, 173–191. doi:10.1016/j.socnet.2006.08.002

- 957 Rosanova, M., Gosseries, O., Casarotto, S., Boly, M., Casali, A. G., Bruno, M.-A., et al. (2012). Recovery
958 of cortical effective connectivity and recovery of consciousness in vegetative patients. *Brain: a journal*
959 *of neurology* 135, 1308–1320. doi:10.1093/brain/awr340
- 960 Rubinov, M. and Sporns, O. (2010). Complex network measures of brain connectivity: uses and
961 interpretations. *NeuroImage* 52, 1059–1069. doi:10.1016/j.neuroimage.2009.10.003
- 962 Rubinov, M. and Sporns, O. (2011). Weight-conserving characterization of complex functional brain
963 networks. *NeuroImage* 56, 2068–2079. doi:10.1016/j.neuroimage.2011.03.069
- 964 Sanz-Arigitá, E. J., Schoonheim, M. M., Damoiseaux, J. S., Rombouts, S. A. R. B., Maris, E., Barkhof, F.,
965 et al. (2010). Loss of ‘small-world’ networks in alzheimer’s disease: graph analysis of fMRI resting-state
966 functional connectivity. *PloS one* 5, e13788. doi:10.1371/journal.pone.0013788
- 967 Schröter, M. S., Spoormaker, V. I., Schorer, A., Wohlschläger, A., Czisch, M., Kochs, E. F., et al. (2012).
968 Spatiotemporal reconfiguration of large-scale brain functional networks during propofol-induced loss of
969 consciousness. *Journal of Neuroscience* 32, 12832–12840
- 970 Schrouff, J., Perlberg, V., Boly, M., Marrelec, G., Boveroux, P., Vanhau denhuys e, A., et al. (2011).
971 Brain functional integration decreases during propofol-induced loss of consciousness. *NeuroImage* 57,
972 198–205. doi:10.1016/j.neuroimage.2011.04.020
- 973 Shadi, K., Bakhshi, S., Gutman, D. A., Mayberg, H. S., and Dovrolis, C. (2016). A symmetry-based method
974 to infer structural brain networks from probabilistic tractography data. *Frontiers in neuroinformatics* 10,
975 46. doi:10.3389/fninf.2016.00046
- 976 Shattuck, D. W., Sandor-Leahy, S. R., Schaper, K. A., Rottenberg, D. A., and Leahy, R. M. (2001).
977 Magnetic resonance image tissue classification using a partial volume model. *NeuroImage* 13, 856–876.
978 doi:10.1006/nimg.2000.0730
- 979 Simpson, S. L., Hayasaka, S., and Laurienti, P. J. (2011). Exponential random graph modeling for complex
980 brain networks. *PloS one* 6, e20039. doi:10.1371/journal.pone.0020039
- 981 Simpson, S. L., Lyday, R. G., Hayasaka, S., Marsh, A. P., and Laurienti, P. J. (2013). A permutation
982 testing framework to compare groups of brain networks. *Frontiers in computational neuroscience* 7, 171.
983 doi:10.3389/fncom.2013.00171
- 984 Simpson, S. L., Moussa, M. N., and Laurienti, P. J. (2012). An exponential random graph modeling
985 approach to creating group-based representative whole-brain connectivity networks. *NeuroImage* 60,
986 1117–1126. doi:10.1016/j.neuroimage.2012.01.071
- 987 Smith, S. M. (2002). Fast robust automated brain extraction. *Human brain mapping* 17, 143–155.
988 doi:10.1002/hbm.10062
- 989 Soddu, A., Vanhau denhuys e, A., Demertzi, A., Bruno, M.-A., Tshibanda, L., Di, H., et al. (2011). Resting
990 state activity in patients with disorders of consciousness. *Functional neurology* 26, 37
- 991 Stamatakis, E. A., Adapa, R. M., Absalom, A. R., and Menon, D. K. (2010). Changes in resting neural
992 connectivity during propofol sedation. *PloS one* 5, e14224. doi:10.1371/journal.pone.0014224
- 993 Sui, J., Pearlson, G., Caprihan, A., Adali, T., Kiehl, K. A., Liu, J., et al. (2011). Discriminating
994 schizophrenia and bipolar disorder by fusing fMRI and DTI in a multimodal CCA+ joint ICA model.
995 *Neuroimage* 57, 97–106. doi:10.1016/j.neuroimage.2011.05.055
- 996 Tallon-Baudry, C. (2009). The roles of gamma-band oscillatory synchrony in human visual cognition.
997 *Frontiers in bioscience (Landmark edition)* 14, 321–332
- 998 Tange, O. (2011). Gnu parallel—the command-line power tool. *The USENIX Magazine* 36, 42–47
- 999 Teasdale, G. and Jennett, B. (1974). Assessment of coma and impaired consciousness: a practical scale.
1000 *The Lancet* 304, 81–84

- 1001 Thengone, D. J., Voss, H. U., Fridman, E. A., and Schiff, N. D. (2016). Local changes in network structure
1002 contribute to late communication recovery after severe brain injury. *Science translational medicine* 8,
1003 368re5–368re5. doi:10.1126/scitranslmed.aaf6113
- 1004 Tollard, E., Galanaud, D., Perlberg, V., Sanchez-Pena, P., Le Fur, Y., Abdennour, L., et al. (2009).
1005 Experience of diffusion tensor imaging and 1H spectroscopy for outcome prediction in severe trau-
1006 matic brain injury: Preliminary results. *Critical care medicine* 37, 1448–1455. doi:10.1097/CCM.
1007 0b013e31819cf050
- 1008 Tononi, G. (2008). Consciousness as integrated information: a provisional manifesto. *The Biological*
1009 *bulletin* 215, 216–242. doi:10.2307/25470707
- 1010 van Wijk, B. C. M., Stam, C. J., and Daffertshofer, A. (2010). Comparing brain networks of different size
1011 and connectivity density using graph theory. *PLoS one* 5, e13701. doi:10.1371/journal.pone.0013701
- 1012 Vanhaudenhuyse, A., Noirhomme, Q., Tshibanda, L. J.-F., Bruno, M.-A., Boveroux, P., Schnakers, C.,
1013 et al. (2010). Default network connectivity reflects the level of consciousness in non-communicative
1014 brain-damaged patients. *Brain: a journal of neurology* 133, 161–171. doi:10.1093/brain/awp313
- 1015 Vincent, J. L., Kahn, I., Snyder, A. Z., Raichle, M. E., and Buckner, R. L. (2008). Evidence for a
1016 frontoparietal control system revealed by intrinsic functional connectivity. *Journal of neurophysiology*
1017 100, 3328–3342. doi:10.1152/jn.90355.2008
- 1018 Voss, H. U., Uluç, A. M., Dyke, J. P., Watts, R., Kobylarz, E. J., McCandliss, B. D., et al. (2006). Possible
1019 axonal regrowth in late recovery from the minimally conscious state. *The Journal of clinical investigation*
1020 116, 2005–2011. doi:10.1172/JCI27021
- 1021 Wang, Y., Ghumare, E., Vandenberghe, R., and Dupont, P. (2017). Comparison of different generalizations
1022 of clustering coefficient and local efficiency for weighted undirected graphs. *Neural computation* 29,
1023 313–331. doi:10.1162/NECO_a.00914
- 1024 Watts, D. J. and Strogatz, S. H. (1998). Collective dynamics of ‘small-world’ networks. *nature* 393, 440
- 1025 Wilson, C. (2010). Aetiological differences in neuroanatomy of the vegetative state: insights from diffusion
1026 tensor imaging and functional implications. *Journal of neurology, neurosurgery, and psychiatry* 81,
1027 475–476. doi:10.1136/jnnp.2010.205815
- 1028 Wu, T., Wang, L., Chen, Y., Zhao, C., Li, K., and Chan, P. (2009). Changes of functional connectivity
1029 of the motor network in the resting state in parkinson’s disease. *Neuroscience letters* 460, 6–10.
1030 doi:10.1016/j.neulet.2009.05.046
- 1031 Yeo, B. T. T., Krienen, F. M., Sepulcre, J., Sabuncu, M. R., Lashkari, D., Hollinshead, M., et al. (2011).
1032 The organization of the human cerebral cortex estimated by intrinsic functional connectivity. *Journal of*
1033 *neurophysiology* 106, 1125–1165. doi:10.1152/jn.00338.2011
- 1034 Zalesky, A., Fornito, A., and Bullmore, E. (2012). On the use of correlation as a measure of network
1035 connectivity. *NeuroImage* 60, 2096–2106. doi:10.1016/j.neuroimage.2012.02.001
- 1036 Zheng, Z. S., Reggente, N., Lutkenhoff, E., Owen, A. M., and Monti, M. M. (2017). Disentangling
1037 disorders of consciousness: Insights from diffusion tensor imaging and machine learning. *Human brain*
1038 *mapping* 38, 431–443. doi:10.1002/hbm.23370
- 1039 Zhou, J., Liu, X., Song, W., Yang, Y., Zhao, Z., Ling, F., et al. (2011). Specific and nonspecific
1040 thalamocortical functional connectivity in normal and vegetative states. *Consciousness and cognition* 20,
1041 257–268. doi:10.1016/j.concog.2010.08.003